

Informing policy via dynamic models: Cholera in Haiti

Jesse Wheeler^{1*}, AnnaElaine L. Rosengart², Zhuoxun Jiang¹, Kevin Tan³, Noah Treutle¹, Edward L. Ionides¹

1 Statistics Department, University of Michigan, Ann Arbor, Michigan, USA

2 Statistics and Data Science, Carnegie Mellon University, Pittsburgh, Pennsylvania, USA

3 Wharton Statistics and Data Science, University of Pennsylvania, Philadelphia, Pennsylvania, USA

* jeswheel@umich.edu

Abstract

Public health decisions must be made about when and how to implement interventions to control an infectious disease epidemic. These decisions should be informed by data on the epidemic as well as current understanding about the transmission dynamics. Such decisions can be posed as statistical questions about scientifically motivated dynamic models. Thus, we encounter the methodological task of building credible, data-informed decisions based on stochastic, partially observed, nonlinear dynamic models. This necessitates addressing the tradeoff between biological fidelity and model simplicity, and the reality of misspecification for models at all levels of complexity. As a case study, we consider the 2010-2019 cholera epidemic in Haiti. We study three dynamic models developed by expert teams to advise on vaccination policies. We assess previous methods used for fitting and evaluating these models, and we develop data analysis strategies leading to improved statistical fit. Specifically, we present approaches to diagnosis of model misspecification, development of alternative models, and computational improvements in optimization, in the context of likelihood-based inference on nonlinear dynamic systems. Our workflow is reproducible and extendable, facilitating future investigations of this disease system.

Author summary

Quantitative understanding of infectious disease transmission dynamics relies upon mathematical models informed by scientific knowledge and relevant data. The models aim to provide a statistical description of the trajectory of an epidemic and its uncertainty, together with a representation of the underlying biological mechanisms. Evaluation of success at these goals is necessary in order for a model to provide a reliable tool for guiding evidence-based public policy interventions. In this article, we discuss common modeling decisions that may not provide an adequate statistical explanation of the data, and we show that attention to statistical fit can lead to more accurate policy evaluations. We do this by conducting a re-analysis of the 2010 cholera outbreak in Haiti. Our analysis presents methodology for diagnosing how well a model describes observed data, and provides careful justification of valid conclusions from the fitted model. Objective measures are used to benchmark model fit; when these are combined with reproducibility, a framework emerges for continual improvement when revisiting the data and models. Our data analysis workflow is supported by recent

advances in algorithms, software and hardware, which facilitate statistical fitting of nonlinear stochastic dynamic models to observed incidence data. However, inference for high-dimensional systems remains a methodological challenge. One of the models under consideration involves spatially coupled stochastic meta-populations, and we demonstrate how a recently developed algorithm permits likelihood-based inference and model diagnostics in this setting. We contend that raising the currently accepted standards of infectious disease modeling will result in a greater ability of scientists and policy makers to understand and respond to future infectious disease outbreaks.

Introduction

Regulation of biological populations is a fundamental topic in epidemiology, ecology, fisheries and agriculture. Population dynamics may be nonlinear and stochastic, with the resulting complexities compounded by incomplete understanding of the underlying biological mechanisms and by partial observability of the system variables. Quantitative models for these dynamic systems offer potential for designing effective control measures. Developing and testing models for dynamic systems, and assessing their fitness for guiding policy, is a challenging statistical task. Questions of interest include: What indications should we look for in the data to assess whether the model-based inferences are trustworthy? What diagnostic tests and model variations can and should be considered in the course of the data analysis? What are the possible trade-offs of increasing model complexity, such as the inclusion of interactions across spatial units?

This case study investigates the use of dynamic models and spatiotemporal data to inform a policy decision in the context of the cholera outbreak in Haiti, which started in 2010. We build on a multi-group modeling exercise by Lee et al. [1] in which four expert modeling teams developed models to the same dataset with the goal of comparing conclusions on the feasibility of eliminating cholera by a vaccination campaign. The data that were used for this study, and that is the subject of our reanalysis, is displayed in Fig. 1. Model 1 is stochastic and describes cholera at the national level; Model 2 is deterministic with spatial structure, and includes transmission via contaminated water; Model 3 is stochastic with spatial structure, and accounts for measured rainfall. Model 4 has an agent-based construction, featuring considerable mechanistic detail but limited ability to calibrate these details to data. We focus on Models 1–3, as the strengths and weaknesses of the agent-based modeling approach [2] are outside the scope of this article.

The four independent teams were given the task of estimating the potential effect of prospective oral cholera vaccine (OCV) programs. While OCV is accepted as a safe and effective tool for controlling the spread of cholera, the global stockpile of OCV doses remains limited [3]. Advances in OCV technology and vaccine availability, however, raised the possibility of planning a national vaccination program [1]. In the study, certain data were shared between the groups, including demography and vaccination history; vaccine efficacy was also fixed at a shared value between groups. Beyond this, the groups made autonomous decisions on what to include and exclude from their models. The groups largely adhered to existing guidelines for creating models to inform policy [4, 5] and, despite their autonomy, obtained a consensus that an extensive nationwide vaccination campaign would be necessary to eliminate cholera from Haiti. Their forecasts, however, were inconsistent with the prolonged period with no confirmed cholera cases between February, 2019 and September, 2022 [6]. Though cholera has recently reemerged in Haiti [7, 8], the inability to accurately forecast cholera incidence from 2019-2022—while diligently adhering to existing scientific standards for infectious disease modeling—demonstrates that existing standards of disease modeling and forecasting may be insufficient.

The discrepancy between the model based conclusions of Lee et al. [1] and the

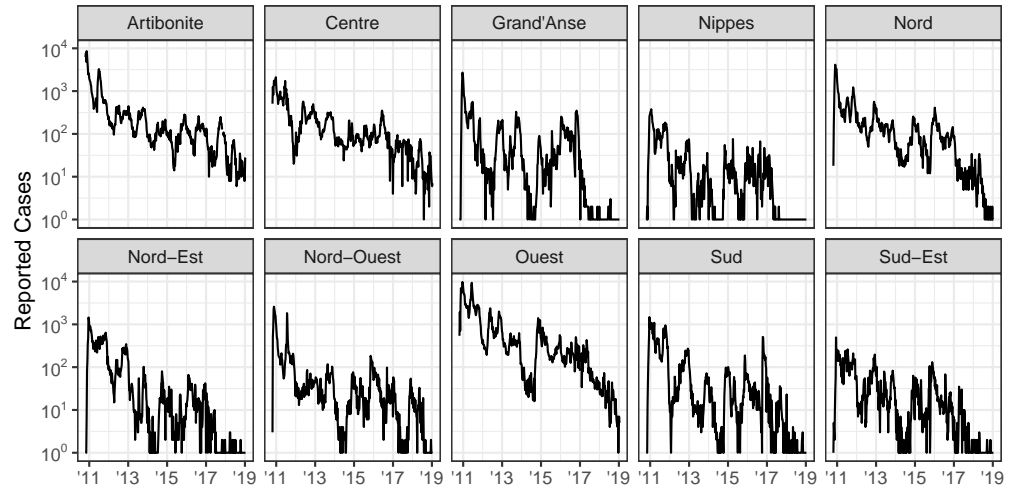


Fig 1. Weekly cholera cases. Weekly reported cholera cases in Haiti from October 2010 to January 2019 for each of the 10 administrative departments.

prolonged absence of cholera in Haiti has been debated [9–12]. Suggested origins of this discrepancy include the use of unrealistic models [10] and unrealistic criteria for cholera elimination [11]. We find a more nuanced conclusion: attention to methodological details in model fitting, diagnosis and forecasting can improve each of the proposed model’s ability to quantitatively describe observed data. This improved ability may result in more accurate forecasts and facilitates the exploration of model assumptions. Based on this retrospective analysis, we offer suggestions on fitting mechanistic models to dynamic systems for future studies.

While this work is focused on the models proposed by Lee et al. [1], our suggestions have broader relevance. To investigate the extent to which [1] is typical of the substantial body of work on Haiti cholera dynamics, we performed a literature review by searching PubMed with keywords: Haiti, cholera, model. The search resulted in 66 papers, of which 32 used dynamic models to describe the cholera epidemic in Haiti. The models make various choices on the dichotomies considered by Lee et al. [1]; deterministic versus stochastic; compartment model versus agent-based; aggregated versus spatially explicit.

We proceed by introducing the general modeling scheme employed by Models 1–3 and provide details of each individual model; we then describe how each model is calibrated to data, and present a systematic approach to examining and refining these models. We then use improved model fits to project cholera incidence in Haiti under various vaccination scenarios considered by Lee et al. [1]. Finally, we conclude with a discussion of the results.

Materials and methods

Mechanistic models for disease modeling

Models that focus on learning relationships between variables in a dataset are called *associative*, whereas models that incorporate a known scientific property of the system are called *causal* or *mechanistic*. The danger in using forecasting techniques which rely on associative models to predict the consequence of interventions is called the Lucas critique in an econometric context. Lucas et al. [13] pointed out that it is naive to

predict the effects of an intervention on a given system based entirely on historical associations. To successfully predict the effect of an intervention, a model should therefore both provide a quantitative explanation of existing data and should have a causal interpretation: a manipulation of the system should correspond quantitatively with the corresponding change to the model. This motivates the development of mechanistic models, which provides a statistical fit to the available data while also supporting a causal interpretation.

The four mechanistic models of Lee et al. [1] were deliberately developed with limited coordination. This allows us to treat the models as fairly independently developed expert approaches to understanding cholera transmission. However, it led to differences in notation, and in subsets of the data chosen for analysis, that hinder direct comparison. Here, we have created a common notational framework that facilitates model comparison, and put all comparable model parameters—including parameters that were estimated or held constant—into Table 1. Translations back to the original notation of Lee et al. [1] are given in the supplement (S1 Table).

Each model describes the cholera dynamics as a partially observed Markov process (POMP) with a latent state vector $\mathbf{X}(t)$ for each continuous time point t . N observations on the system are collected at time points t_1, \dots, t_N , written as $t_{1:N}$. The observation at time t_n is modeled by the random vector \mathbf{Y}_n . While the latent process exists between observation times, the value of the latent state at observations times is of particular interest. We therefore write $\mathbf{X}_n = \mathbf{X}(t_n)$ to denote the value of the latent process at the n th observation time, and $\mathbf{X}_{1:N}$ is the collection of latent state values for all observed time points. The observable random variables $\mathbf{Y}_{1:N}$ are assumed to be conditionally independent given $\mathbf{X}_{0:N}$. Together, with the density for the initial value of the latent state $\mathbf{X}_0 = \mathbf{X}(t_0)$, each model assumes a joint density $f_{\mathbf{X}_{0:N}, \mathbf{Y}_{1:N}}(\mathbf{x}_{0:N}, \mathbf{y}_{1:N}; \theta)$, where θ is a parameter vector that indexes the model. The observed data $\mathbf{y}_{1:N}^*$, along with the unobserved true value of the latent state, are modeled as a realization of this joint distribution.

Because of the probabilistic nature of both the unobserved latent state and the observable random variables, it is possible to consider various marginal and conditional densities of these two jointly random vectors. An important example is the marginal density of the observed random vector $\mathbf{Y}_{1:N}$, evaluated at the observed data $\mathbf{y}_{1:N}^*$, as shown in Eq. (1):

$$f_{\mathbf{Y}_{1:N}}(\mathbf{y}_{1:N}^*; \theta) = \int f_{\mathbf{X}_{0:N}, \mathbf{Y}_{1:N}}(\mathbf{x}_{0:N}, \mathbf{y}_{1:N}; \theta) d\mathbf{x}_{0:N}. \quad (1)$$

When treated as a function of the parameter vector θ , this marginal density is called the *likelihood function*, which is the basis of likelihood based statistical inference.

Using the conditional independence of $\mathbf{Y}_{1:N}$ given $\mathbf{X}_{0:N}$ and the Markov property of $\mathbf{X}_{0:N}$, the joint density can be refactored into the useful form given in Eq. (2):

$$f_{\mathbf{X}_{0:N}, \mathbf{Y}_{1:N}}(\mathbf{x}_{0:N}, \mathbf{y}_{1:N}; \theta) = f_{\mathbf{X}_0}(\mathbf{x}_0; \theta) \prod_{n=1}^N f_{\mathbf{X}_n | \mathbf{X}_{n-1}}(\mathbf{x}_n | \mathbf{x}_{n-1}; \theta) f_{\mathbf{Y}_n | \mathbf{X}_n}(\mathbf{y}_n | \mathbf{x}_n). \quad (2)$$

This factorization is useful because it demonstrates that POMP models may be completely described using three parts: the *initialization model* for the latent states $f_{\mathbf{X}_0}(\mathbf{x}_0; \theta)$; the *one-step transition density*, or the *process model* $f_{\mathbf{X}_n | \mathbf{X}_{n-1}}(\mathbf{x}_n | \mathbf{x}_{n-1}; \theta)$; and the *measurement model* $f_{\mathbf{Y}_n | \mathbf{X}_n}(\mathbf{y}_n | \mathbf{x}_n)$. In the following subsections, we describe Models 1–3 in terms of these three components. The latent state vector $\mathbf{X}(t)$ for each model consists of individuals labeled as susceptible (S), infected (I), asymptotically infected (A), vaccinated (V), and recovered (R), with various sub-divisions sometimes

Table 1. Model parameters.

Mechanism	Model 1	Model 2	Model 3
Infection (day)	$\mu_{IR}^{-1} = 2.0^\dagger$ (8)	$\mu_{IR}^{-1} = 7.0^\dagger$ (16)	$\mu_{IR}^{-1} = 5.0^\dagger$ (28)
Latency (day)	$\mu_{EI}^{-1} = 1.4^\dagger$ (7)	$\mu_{EI}^{-1} = 1.3^\dagger$ (15)	
Seasonality	$\beta_{1:6} = (1.6, 1.1, 1.3, 1.1, 1.5, 0.9)$ (4) $\zeta = -0.06^*$ (34)	$a = 0.4^\dagger$ (13) $\phi = 7.26^*$ (13)	$a = 2.07$ (32) $r = 1.21$ (32)
Immunity (yr)	$\mu_{RS}^{-1} = 8.0^\dagger$ (9)	$\mu_{RS}^{-1} = 3.3 \times 10^{12}$ (17) $\omega_1^{-1} = 1.0^\dagger$ (19) $\omega_2^{-1} = 5.0^\dagger$ (20)	$\mu_{RS}^{-1} = 8.0^\dagger$ (30)
Birth/death (yr ⁻¹)	$\mu_S = 10^{-2} \times 2.23^\dagger$ (11) $\delta = 10^{-3} \times 7.5^\dagger$ (11)		$\delta = 10^{-2} \times 1.59^\dagger$ (29) $\delta_C = 1.46^\dagger$
Sympt. frac.	$f_z(t) = c\vartheta^*(t - \tau_d)^\dagger$ (6-7)	$f = 0.2^\dagger$ (15)	$f = 0.25^\dagger$ (27)
Asympt. infectivity	$\epsilon = 0.05^\dagger$ (3)	$\epsilon = 0.001^\dagger$ (13) $\epsilon_W = 10^{-7^\dagger}$ (21)	$\epsilon = 1^\dagger$ (25) $\epsilon_W = 0.081$ (32)
Human to human	$\beta_{1:6}$ as above (3)	$\beta = 3.85 \times 10^{-16}$ (13)	$\beta_{1:10} = (0.43, 0.17, 0.30, 0.13, 0.35, 0.39, 0.20, 0.03, 0.30, 0.21) \times 10^{-6}$ (25)
Water to human		$W_{\text{sat}} = 10^{5^\dagger}$ (13) $\beta_W = 1.1$ (13)	$\beta_{W_{1:10}} = (4.15, 18.45, 21.40, 22.43, 4.50, 25.37, 9.55, 0.86, 10.01, 10.27)$ (25)
Human to water		$\mu_W = 9340$ (21)	$\mu_W = 5.79 \times 10^{-5}$ (32)
Water survival (wk)		$\delta_W^{-1} = 3^\dagger$ (22)	$\delta_W^{-1} = 0.10$ (33)
Mixing exponent	$\nu = 0.97$ (3)		
Process noise (wk ^{1/2})	$\sigma_{\text{proc}} = (0.31, 0.35)^*$ (3)		$\sigma_{\text{proc}} = 0.028$ (27)
Reporting rate	$\rho = 0.898$ (S15)	$\rho = 0.20^\dagger$ (S16)	$\rho = 0.87$ (S19)
Observation variance	$\psi = (356.16, 59.55)$ (S15)	$\psi = 3.05 \times 10^{-13}$ (S16)	$\psi = 169.53$ (S19)
Initial Values	$I_{0,0} = 5284$ $E_{0,0} = 89$		$I_{0,0}^{3,4} = (2, 12)^*$ (S20)
Hurricane Parameters			$\beta_{W_{3,9}}^{hm} = (27.48, 22.75)^*$ (25) $h_{3,9}^{hm} = (102.47, 83.48)^*$ (25)

References to the relevant equation are given in parentheses. Parameters that were fixed and not calibrated using the data are indicated with \dagger ; all fixed parameters values were chosen to match the fixed parameter values of [1]. Parameters that were added during our re-analysis and were not considered by Lee et al. are indicated with $*$. Translations back into the notation of [1] are given in S1 Table.

considered. The observable random vector $\mathbf{Y}_{1:N}$ represents the random vector of cholera incidence data for each model; Models 2 and 3 have metapopulation structure, meaning that each individual is a member of a spatial unit, denoted by a subscript $u \in 1:U$, in which case we denote the observed data for each unit using $\mathbf{y}_{1:N}^* = \mathbf{y}_{1:N,1:U}^*$. Here, the spatial units are the $U = 10$ Haitian administrative départements (henceforth anglicized as departments).

While the complete model description is scientifically critical, as well as necessary for transparency and reproducibility, the model details are not essential to our methodological discussions of how to diagnose and address model misspecification with the purpose of informing policy. A first-time reader may choose to skim through the rest of this section, and return later. Additional details about the numeric implementation of these models are provided in a supplemental text (S1 Text). While each of the dynamic models considered in this manuscript can be fully described using the mathematical equations provided in the following section, diagrams of dynamic systems can be helpful to understand the equations. For this reason, we provide flow chart diagrams for Models 1–3 in supplement figures (S1 Fig, S2 Fig and S3 Fig).

Model 1

The latent state vector $\mathbf{X}(t) = (S_z(t), E_z(t), I_z(t), A_z(t), R_z(t), z \in 0:Z)$ describes susceptible, latent (exposed), infected (and symptomatic), asymptomatic, and recovered individuals in vaccine cohort z at time t . Here, $z = 0$ corresponds to unvaccinated individuals, and $z \in 1:Z$ describes hypothetical vaccination programs. The force of infection is

$$\lambda(t) = \left(\sum_{z=0}^Z I_z(t) + \epsilon \sum_{z=0}^Z A_z(t) \right)^\nu \frac{d\Gamma(t)}{dt} \beta(t) / N, \quad (3)$$

where $\beta(t)$ is a periodic cubic spline representation of seasonality, given in terms of a B-spline basis $\{s_j(t), j \in 1:6\}$ and parameters $\beta_{1:6}$ as

$$\log \beta(t) = \sum_{j=1}^6 \beta_j s_j(t). \quad (4)$$

The process noise $d\Gamma(t)/dt$ is multiplicative Gamma-distributed white noise, with infinitesimal variance parameter σ_{proc}^2 . Lee et al. [1] included process noise in Model 3 but not in Model 1, i.e., they fixed $\sigma_{\text{proc}}^2 = 0$. Gamma white noise in the transmission rate gives rise to an over-dispersed latent Markov process [14] which has been found to improve the statistical fit of disease transmission models [15, 16].

For any time point in $t_{1:N}$, the process model $f_{\mathbf{X}_n | \mathbf{X}_{n-1}}(\mathbf{x}_n | \mathbf{x}_{n-1}; \theta)$ is defined by the describing how individuals move from one latent state compartment to another. Per-capita transition rates are given in Eqs. (5)-(12):

$$\mu_{S_z E_z} = \lambda(t), \quad (5)$$

$$\mu_{E_z I_z} = \mu_{EI} (1 - \vartheta_z(t)), \quad (6)$$

$$\mu_{E_z A_z} = \mu_{EI} \vartheta_z(t), \quad (7)$$

$$\mu_{I_z R_z} = \mu_{A_z R_z} = \mu_{IR}, \quad (8)$$

$$\mu_{R_z S_z} = \mu_{RS}, \quad (9)$$

$$\mu_{S_0 S_z} = \mu_{E_0 E_z} = \mu_{I_0 I_z} = \mu_{A_0 A_z} = \mu_{R_0 R_z} = \eta_z(t), \quad (10)$$

$$\mu_{S_z \bullet} = \mu_{E_z \bullet} = \mu_{I_z \bullet} = \mu_{A_z \bullet} = \mu_{R_z \bullet} = \delta, \quad (11)$$

$$\mu_{\bullet S_0} = \mu_S, \quad (12)$$

where $z \in 0:Z$. Here, μ_{AB} is a transition rate from compartment A to B . We have an additional demographic source and sink compartment \bullet modeling entry into the study population due to birth or immigration, and exit from the study population due to death or immigration. Thus, $\mu_{A\bullet}$ is a rate of exiting the study population from compartment A and $\mu_{\bullet B}$ is a rate of entering the study population into compartment B .

In Model 1, the advantage afforded to vaccinated individuals is an increased probability that an infection is asymptomatic. Conditional on infection status, vaccinated individuals are also less infectious than their non-vaccinated counterparts by a rate of $\epsilon = 0.05$ in Eq. (3). In Eqs. (7) and (6) the asymptomatic ratio for non-vaccinated individuals is set $f_0(t) = 0$, so that the asymptomatic route is reserved for vaccinated individuals. For $z \in 1:Z$, the vaccination cohort z is assigned a time τ_z , and we take $\vartheta_z(t) = c\vartheta^*(t - \tau_z)$ where $\vartheta^*(t)$ is efficacy at time t since vaccination for adults, taken from [1], Table S4, and $c = (1 - (1 - 0.4688) \times 0.11)$ is a correction to allow for reduced efficacy in the 11% of the population aged under 5 years. Single and double vaccine doses were modeled by changing the waning of protection; protection was modeled as equal between single and double dose until 52 weeks after vaccination, at which point the single dose becomes ineffective.

The latent state vector $\mathbf{X}(t)$ is initialized by setting the counts for each compartment and vaccination scenario $z \neq 0$ as zero, and introducing initial-value parameters $I_{0,0}$ and $E_{0,0}$ such that $R_0(0) = 0$, $I_0(0) = \text{Pop} \times I_{0,0}$, $E_0(0) = \text{Pop} \times E_{0,0}$ and $S_0(0) = \text{Pop} \times (1 - I_{0,0} - E_{0,0})$, where Pop is the total population of Haiti. The measurement model describes reported cholera cases at time point n come from a negative binomial distribution, where only a fraction (ρ) of new weekly cases are reported. More details about the initialization model $f_{\mathbf{X}_0}(\mathbf{x}_0; \theta)$ and the *measurement model* $f_{\mathbf{Y}_n|\mathbf{X}_n}(\mathbf{y}_n|\mathbf{x}_n)$ for Models 1–3 are provided a supplement text (S2 Text and S3 Text).

Model 2

Susceptible individuals are in compartments $S_{uz}(t)$, where $u \in 1:U$ corresponds to the $U = 10$ departments, and $z \in 0:4$ describes vaccination status:

$z = 0$: Unvaccinated or waned vaccination protection.

$z = 1$: One dose at age under five years.

$z = 2$: Two doses at age under five years.

$z = 3$: One dose at age over five years.

$z = 4$: Two doses at age over five years.

Like Model 1, the process model $f_{\mathbf{X}_n|\mathbf{X}_{n-1}}(\mathbf{x}_n|\mathbf{x}_{n-1}; \theta)$ is primarily defined via the description of movement of individuals between compartments, however Model 2 also includes a dynamic description of a latent bacterial compartment as well. Individuals can progress to a latent infection E_{uz} followed by symptomatic infection I_{uz} with recovery to R_{uz} or asymptomatic infection A_{uz} with recovery to R_{uz}^A . The force of infection depends on both direct transmission and an aquatic reservoir, $W_u(t)$, and is given by

$$\lambda_u(t) = 0.5(1 + a \cos(2\pi t + \phi)) \frac{\beta_W W_u(t)}{W_{\text{sat}} + W_u(t)} + \beta \left\{ \sum_{z=0}^4 I_{uz}(t) + \epsilon \sum_{z=0}^4 A_{uz}(t) \right\}. \quad (13)$$

The latent state is therefore described by the vector $\mathbf{X}(t) = (S_{uz}(t), E_{uz}(t), I_{uz}(t), A_{uz}(t), R_{uz}(t), R_{uz}^A(t), W_u, u \in 1:U, z \in 0:4)$. The cosine term in Eq. (13) accounts for

annual seasonality, with a phase parameter ϕ . The Lee et al. [1] implementation of Model 2 fixes $\phi = 0$.

Individuals move from department u to v at rate T_{uv} , and aquatic cholera moves at rate T_{uv}^W . The nonzero transition rates are

$$\mu_{S_{uz}E_{uz}} = \vartheta_z \lambda, \quad (14)$$

$$\mu_{E_{uz}I_{uz}} = f\mu_{EI}, \quad \mu_{E_{uz}A_{uz}} = (1-f)\mu_{EI}, \quad (15)$$

$$\mu_{I_{uz}R_{uz}} = \mu_{A_{uz}R_{uz}^A} = \mu_{IR}, \quad (16)$$

$$\mu_{R_{uz}S_{uz}} = \mu_{R_{uz}^A S_{uz}} = \mu_{RS}, \quad (17)$$

$$\mu_{S_{uz}S_{vz}} = \mu_{E_{uz}E_{vz}} = \mu_{I_{uz}I_{vz}} = \mu_{A_{uz}A_{vz}} = \mu_{R_{uz}R_{vz}} = \mu_{R_{uz}^A R_{vz}^A} = T_{uv}, \quad (18)$$

$$\mu_{S_{u1}S_{u0}} = \mu_{S_{u3}S_{u0}} = \omega_1, \quad (19)$$

$$\mu_{S_{u2}S_{u0}} = \mu_{S_{u4}S_{u0}} = \omega_2, \quad (20)$$

$$\mu_{\bullet W_u} = \mu_W \left\{ \sum_{z=0}^4 I_{uz}(t) + \epsilon_W \sum_{z=0}^4 A_{uz}(t) \right\}, \quad (21)$$

$$\mu_{W_u \bullet} = \delta_W, \quad (22)$$

$$\mu_{W_u W_v} = w_r T_{uv}^W. \quad (23)$$

In Eq. (18) the spatial coupling is specified by a gravity model,

$$T_{uv} = v_{\text{rate}} \times \frac{\text{Pop}_u \text{Pop}_v}{D_{uv}^2}, \quad (24)$$

where Pop_u is the mean population for department u , D_{uv} is a distance measure estimating average road distance between randomly chosen members of each population, and $v_{\text{rate}} = 10^{-12} \text{ km}^2 \text{ yr}^{-1}$ was treated as a fixed constant. In Eq. (23), T_{uv}^W is a measure of river flow between departments. The unit of $W_u(t)$ is cells per ml, with dose response modeled via a saturation constant of W_{sat} in Eq. (13). In Eq. (14), ϑ_z denotes the vaccine efficacy for each vaccination campaign $z \in Z$, with $\vartheta_0 = 1$, $\vartheta_1 = 1 - 0.429q$, $\vartheta_2 = 1 - 0.519q$, $\vartheta_3 = 1 - 0.429$, and $\vartheta_4 = 1 - 0.519$. Here, $q = 0.4688$ represents the reduced efficacy of the vaccination for children under the age of five years, and the values 0.429 and 0.519 are the median effectiveness of one and two doses over their effective period respectively, according to Table S4 in the supplement material of Lee et al. [1]. Because vaccine efficacy remains constant, individuals in this model transition from a vaccinated compartment to the susceptible compartment at the end of the vaccine coverage period.

The starting value for each element of the latent state vector $\mathbf{X}(0)$ are set to zero except for $I_{u0}(0) = y_u^*(0)/\rho$ and $R_{u0}(0) = \text{Pop}_u - I_{u0}(0)$, where $y_u^*(0)$ is the reported number of cholera cases in department u at time $t = 0$. Reported cases are described using a log-normal distribution, with the log-scale mean equal to the reporting rate ρ times the number of newly infected individuals. See the section describing how Model 2 is fit to data and Sec. S3.2 of the supplement for more details.

Model 3

The latent state is described as $\mathbf{X}(t) = (S_{uz}(t), I_u(t), A_u(t), R_{uzk}(t), W_u(t), u \in 0:U, z \in 0:4, k \in 1:3)$. Here, $z = 0$ corresponds to unvaccinated, $z = 2j - 1$ corresponds to a single dose on the j th vaccination campaign in unit u and $z = 2j$ corresponds to receiving two doses on the j th vaccination campaign. $k \in 1:3$ models non-exponential duration in the recovered class before waning of immunity. The processes model $f_{\mathbf{X}_n | \mathbf{X}_{n-1}}(\mathbf{x}_n | \mathbf{x}_{n-1}; \theta)$ describes the movement of individuals between latent

compartments, as well as the birth and death process of local, unobserved bacterial compartments $W_u(t)$. The force of infection is

$$\lambda_u(t) = \left(\beta_{W_u} + \mathbf{1}_{(t \geq t_{hm})} \beta_{W_u}^{hm} e^{-h_u^{hm}(t-t_{hm})} \right) \frac{W_u(t)}{1 + W_u(t)} + \beta_u \sum_{v \neq u} (I_v(t) + \epsilon A_v(t)), \quad (25)$$

where t_{hm} is the time Hurricane Matthew struck Haiti [17], and $\mathbf{1}_{(A)}$ is the indicator function for event A . In [1], $\beta_{W_u}^{hm}$ and h_u^{hm} were set to zero for all u ; the need to account for the effect Hurricane Matthew had on cholera transmission for this model is explored in Sec. S5 of the supplement.

Per-capita transition rates are used for both compartments representing human counts and the aquatic reservoir of bacteria; these rates are given in Eqs. (26)–(33).

$$\mu_{S_{uz}I_u} = f \lambda_u (1 - \vartheta_{uz}(t)) d\Gamma/dt, \quad (26)$$

$$\mu_{S_{uz}A_u} = (1 - f) \lambda_u (1 - \vartheta_{uz}(t)) d\Gamma/dt, \quad (27)$$

$$\mu_{I_u R_{uz1}} = \mu_{A_u R_{uz1}} = \mu_{IR}, \quad (28)$$

$$\mu_{I_u S_{u0}} = \delta + \delta_C, \quad \mu_{A_u S_{u0}} = \delta \quad (29)$$

$$\mu_{R_{uz1} R_{uz2}} = \mu_{R_{uz2} R_{uz3}} = 3\mu_{RS}, \quad (30)$$

$$\mu_{R_{uzk} S_{u0}} = \delta + 3\mu_{RS} \mathbf{1}_{\{k=3\}}, \quad (31)$$

$$\mu_{\bullet W_u} = [1 + a(J_u(t))^r] \text{Den}_u \mu_W [I_u(t) + \epsilon W A_u(t)], \quad (32)$$

$$\mu_{W_u \bullet} = \delta_W. \quad (33)$$

As with Model 1, $d\Gamma_u(t)/dt$ is multiplicative Gamma-distributed white noise in Eqs. (26) and (27). In Eq. (32), $J_u(t)$ is a dimensionless measurement of precipitation that has been standardized by dividing the observed rainfall at time t by the maximum recorded rainfall in department u during the epidemic, and Den_u is the population density. Demographic stochasticity is accounted for by modeling non-cholera related death rate δ in each compartment, along with an additional death rate δ_C in Eq. (29) to account for cholera induced deaths among infected individuals. All deaths are balanced by births into the susceptible compartment in Eqs. (29) and (31), thereby maintaining constant population in each department.

Similar to Model 1, there are no distinct compartments for individuals under five years of age, and the vaccination efficacy is taken as a age adjusted weighted average of the efficacy for individuals both over and under five years of age: $\vartheta_{uz}(t) = c\vartheta^*(t - \tau_{uz})$, where τ_{uz} is the vaccination time for unit u and vaccination campaign z . The value c and the function ϑ^* are equivalent to those described in the Model 1 description.

Latent states are initialized using an approximation of the instantaneous number of infected, asymptomatic, and recovered individuals at time t_0 by using the first week of cholera incidence data. Specifically, we set $I_{u0}(0) = \frac{y_{1u}^*}{\rho(\delta + \delta_C + \mu_{IR})}$, $A_{u0}(0) = \frac{1-f}{f} I_{u0}(0)$, $R_{u0k} = y_{1u}^* - I_{u0}(0) - A_{u0}(0)$, and we initialize $W_u(0)$ by enforcing the rainfall dynamics supposed by the one step transition model; all other compartments that represent population counts are set to zero at time t_0 . For each unit u with zero case counts at time t_1 , this initialization scheme results in having zero individuals in the Infected and Asymptomatic compartments, as well as having no bacteria in the aquatic reservoir. In reality, it is plausible that some bacteria or infected individuals were present in unit u but went unreported. Therefore, for departments with zero case counts in week 1, we consider estimating the number of infected individuals rather than treating this value as a constant (see supplement Sec. S5 for more details). Finally, reported cholera cases are modeled using a negative binomial measurement model with mean equal to a fraction (ρ) of individuals in each unit who develop symptoms and seek healthcare (see Sec. S3.3 of the supplement).

Model Fitting

Each of the three models considered in this study describes cholera dynamics as a partially observed Markov process (POMP), with the understanding that the deterministic Model 2 is a degenerate case of a stochastic model. Each model is indexed by a parameter vector, θ , and different values of θ can result in qualitative differences in the predicted behavior of the system. Therefore, the choice of θ used to make inference about the system can greatly affect model based conclusions. Elements of θ can be fixed at a constant value based on scientific understanding of the system, but parameters can also be calibrated to data by maximizing a measure of congruency between the observed data and the model’s mechanistic structure. Calibrating model parameters to observed data does not guarantee that the resulting model successfully approximates real-world mechanisms, since the model description of the dynamic system may be incorrect and do not change as the model is calibrated to data. However, the congruency between the model and observed data serves as a proxy for the congruency between the model and the true underlying dynamic system. As such, it is desirable to obtain the best possible fit of the proposed mechanistic structure to the observed data.

In this article we calibrate the parameters of each of our models by maximizing the likelihood, as described in Eq. (1). The likelihood for each of the fitted models—and the corresponding AIC values for model comparisons that include an adjustment for the number of calibrated parameters—is provided in Table 2. In the following subsections we describe in detail our approach to calibrating the three proposed mechanistic models to observed cholera incidence data.

Table 2. AIC values for Models 1–3 and their benchmarks.

	Model 1	Model 2	Model 3
Log-likelihood	−2731.3 (−3030.9) ¹	−21957.3 (−29367.4)	−17402.4 (−33832.6) ²
Number of Fit Parameters	15 (20)	6 (6)	34 (29)
AIC	5492.7 (6101.8) ¹	43926.5 (58746.9)	34872.8 (67723.2) ²
Benchmark AIC	5585.3	36961.0	37108.0

Values in parentheses are corresponding values using Lee et al. [1] parameter estimates. ¹The reported likelihood is an upper bound of the likelihood of the Lee et al. [1] model. ²Lee et al. [1] fit Model 3 to a subset of the data (March 2014 onward, excluding data from Ouest in 2015-2016). On this subset, their model has a likelihood of −9721.2. On this same subset, our model has a likelihood of −7236.5. Details of estimating the likelihood of the Lee et al. [1] models is provided in S4 Text See Sec. S6 of the supplement material for more details on estimating the likelihood of the Lee et al. [1] models.

Calibrating Model 1 Parameters

Model 1 was developed with the intent of providing a description of cholera dynamics that is scientifically plausible rather than one that is statistically convenient. This results in the inability to obtain a closed form expression of the non-linear joint model density—described in Eq. (2). Therefore in order to perform likelihood based inference on this model, we are restricted to use parameter estimation techniques that have the

plug-and-play property, which is that the fitting procedure only requires the ability to simulate the latent process rather than evaluating transition densities [16, 18]; in the context of the notation and definitions employed in this article, this means that we only require the ability to simulate from $f_{\mathbf{X}_0}(\mathbf{x}_0; \theta)$ and $f_{\mathbf{X}_n | \mathbf{X}_{n-1}}(\mathbf{x}_n | \mathbf{x}_{n-1}; \theta)$ rather than needing to evaluate these densities. Plug-and-play algorithms include Bayesian approaches like ABC and PMCMC [19, 20], but here we use algorithms that enable maximum likelihood estimation. To our knowledge, the only plug-and-play methods that can be used to maximize the likelihood for POMP models of this complexity are iterated filtering algorithms [21], which modify the well-known *particle filter* [22].

The particle filter, also referred to as sequential Monte Carlo, is a simulation based method that is frequently used in Bayesian inference to approximate the posterior distribution of latent states. This algorithm can also be used to accurately approximate the log-likelihood of a POMP model, defined as the integral in Eq. (1). Iterated filtering—algorithms such as IF2 [21]—extend the particle filter by performing a random walk for each parameter and particle; these perturbations are carried out iteratively over multiple filtering operations, using the collection of parameters from the previous filtering pass as the parameter initialization for the next iteration, and decreasing the random walk variance at each step. With a sufficient number of iterations, the resulting parameter values converge to a region of the parameter space that maximizes the model likelihood.

The ability to maximize the likelihood allows for likelihood-based inference, such as performing statistical tests for potential model improvements. We demonstrate this capability by proposing a linear trend ζ in transmission in Eq. (4):

$$\log \beta(t) = \sum_{j=1}^6 \beta_s s_j(t) + \zeta \bar{t}, \quad (34)$$

where $\bar{t} = \frac{t - (t_N + t_0)/2}{t_N - (t_N + t_0)/2}$, so that $\bar{t} \in [-1, 1]$. The proposal of a linear trend in transmission is a result of observing an apparent decrease in reported cholera infections from 2012-2019 in Fig. 1. While several factors may contribute to this decrease, one explanation is that case-area targeted interventions (CATIs), which included education sessions, increased monitoring, household decontamination, soap distribution, and water chlorination in infected areas [23], may have substantially reduced cholera transmission over time [24].

We perform a statistical test to determine whether or not the data indicate the presence of a linear trend in transmissibility. To do this, we perform a profile-likelihood search on the parameter ζ and obtain a 95% confidence interval via a Monte Carlo Adjusted Profile (MCAP) [25]. Lee et al. [1] implemented Model 1 by fitting two distinct phases: an epidemic phase from October 2010 through March 2015, and an endemic phase from March 2015 onward. We similarly allow the re-estimation of process and measurement overdispersion parameters (σ_{proc}^2 and ψ), and require that the latent Markov process $X(t)$ carry over from one phase into the next. The resulting confidence interval for ζ is $(-0.085, -0.005)$, with the full results displayed in Fig. 2. These results are suggestive that the inclusion of a trend in the transmission rate improves the quantitative ability of Model 1 to describe the observed data. The reported results for Model 1 in the remainder of this article were obtained with the inclusion of the parameter ζ .

If a mechanistic model including a feature (such as a representation of a mechanism, or the inclusion of a covariate) fits better than mechanistic models without that feature, and also has competitive fit compared to associative benchmarks, this may be taken as evidence supporting the scientific relevance of the feature. As for any analysis of observational data, we must be alert to the possibility of confounding. For a covariate,

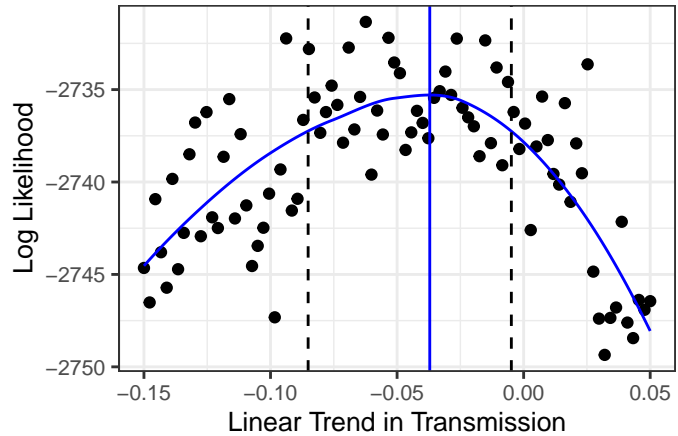


Fig 2. Confidence interval for linear trend in transmission. Monte Carlo adjusted profile of ζ for Model 1. The blue curve is the profile, the blue line indicates the MLE, and the dashed lines indicate the 95% confidence interval.

this shows up in a similar way to regression analysis: the covariate under investigation could be a proxy for some other unmodeled or unmeasured covariate. For a mechanism, the model feature could in principle explain the data by helping to account for some different unmodeled phenomenon. The statistical evidence of a trend in transmission rate in this model could be explained by any trending variable (such as hygiene improvements, or changes in population behavior), resulting in confounding from collinear covariates. Alternatively, the trend could be attributed to a decreasing reporting rate rather than decreasing transmission rate, resulting in confounded mechanisms. The robust statistical conclusion is that a model which allows for change fits better than one which does not—we argue that a decreasing transmission rate is a plausible way to explain this, but the incidence data themselves do not provide enough information to pin down the mechanism.

We implemented Model 1 using the `pomp` package [26], relying heavily on the `pomp` source code provided by Lee et al. [1]. Both analyses used the `mif2` implementation of the IF2 algorithm to estimate θ by maximum likelihood. One change we made in the statistical analysis that led to larger model likelihoods was increasing the computational effort in the numerical maximization. While IF2 enables parameter estimation for a large class of models, the theoretic ability to maximize the likelihood depends on asymptotics in both the number of particles and the number of filtering iterations. Many Monte Carlo replications are then required to quantify and further reduce the error. The large increase in the log-likelihood for Model 1 (see Table 2) can primarily be attributed to increasing the computational effort in fitting the model; this result highlights the importance of carefully determining the necessary computational effort needed to maximize model likelihoods and acting accordingly. Simulations from the initial conditions of our fitted model are plotted against the observed incidence data in Fig. 3.

Calibrating Model 2 Parameters

Model 2 is a deterministic compartmental model defined by a set of coupled differential equations. The use of deterministic compartment models have a long history in the field of infectious disease epidemiology [27–29], and can be justified by asymptotic considerations in a large-population limit [30,31]. Because the process model of Model 2 is deterministic, maximum likelihood estimation reduces to a least squares calculation

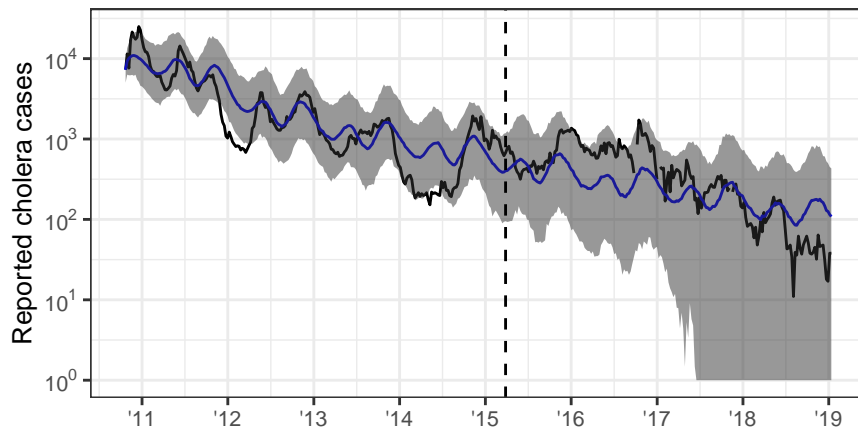


Fig 3. Simulations from Model 1 compared to reported cholera cases. The black curve is observed data, the blue curve is median of 500 simulations from the fitted model, and the vertical dashed line represents break-point when parameters are refit.

when combined with a Gaussian measurement model (see Sec. S3.2 of the supplement material for details). Lee et al. [1] fit two versions of Model 2 based on a presupposed change in cholera transmission from an epidemic phase to endemic phase that occurred in March, 2014. The inclusion of a change-point in model states and parameters increases the flexibility of the model and hence the ability to fit the observed data. The increase in model flexibility, however, results in hidden states that are inconsistent between model phases. The inclusion of a model break-point by Lee et al. [1] is perhaps due to a challenging feature of fitting a deterministic model via least squares: discrepancies between model trajectories and observed case counts in highly infectious periods of a disease outbreak will result in greater penalty than the discrepancies between model trajectories and observed case counts in times of relatively low infectiousness, resulting in a bias towards accurately describing periods of high infectiousness. This issue is particularly troublesome for modeling cholera dynamics in Haiti: the inability to accurately fit times of low infectiousness may result in poor model forecasts, as few cases of cholera were observed in the last few years of the epidemic.

To combat this issue, we fit the model to log-transformed case counts, since the log scale stabilizes the variation during periods of high and low incidence. An alternative solution is to change the measurement model to include overdispersion, as was done in Models 1 and 3. This permits the consideration of demographic stochasticity, which is dominant for small infected populations, together with log scale stochasticity (also called multiplicative, or environmental, or extra-demographic) which is dominant at high population counts. Here we chose to fit the model to transformed case counts rather than adding overdispersion to the measurement model with the goal of minimizing the changes to the model proposed by Lee et al. [1].

We implemented this model using the `spatPomp` R package [32]. The model was then fit using the subplex algorithm, implemented in the `subplex` package [33]. A comparison of the trajectory of the fitted model to the data is given in Fig. 4.

Calibrating Model 3 Parameters

Model 3 describes cholera dynamics in Haiti using a metapopulation model, where the hidden states in each administrative department has an effect on the dynamics in other departments. The decision to address metapopulation dynamics using a spatially explicit model, rather than to aggregate over space, is double-edged. Evidence for the

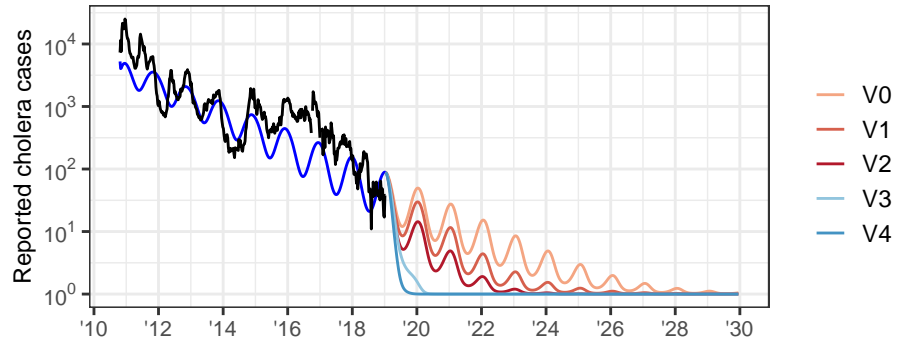


Fig 4. Simulated trajectory of Model 2. The black line shows the nationally aggregated weekly cholera incidence data. The blue curve from 2012-2019 is the trajectory of the calibrated version of Model 2. Projections under the various vaccination scenarios, which are discussed in detail in the **Forecasts** subsection are also included.

former approach has been provided in previous studies [34], including the specific case of heterogeneity between Haitian departments in cholera transmission [35]. However, a legitimate preference for simplicity can support a decision to consider nationally aggregated models [5,36]. One issue that arises when fitting spatially explicit models is that parameter estimation techniques based on the particle filter become computationally intractable as the number of spatial units increases. This is a result of the approximation error of particle filters growing exponentially in the dimension of the model [37,38].

To avoid the approximation error present in high-dimensional models, Lee et al. [1] simplified the problem of estimating the parameters of Model 3 by creating an approximate version of the model where the units are independent given the observed data. Reducing a spatially coupled model to individual units in this fashion requires special treatment of any interactive mechanisms between spatial units, such as found in Eq. (25). Because the simplified, spatially-decoupled version of Model 3 implemented in [1] relies on the observed cholera cases, the calibrated model cannot readily be used to obtain forecasts. Therefore, in order to obtain model forecasts, Lee et al. [1] used the parameters estimates from the spatially-decoupled approximation of Model 3 to obtain forecasts using the fully coupled version of the model. This approach of model calibration and forecasting avoids the issue of particle depletion, but may also be problematic. One concern is that cholera dynamics in department u are highly related to the dynamics in the remaining departments; calibrating model parameters while conditioning on the observed cases in other departments may therefore lead to an over-dependence on observed cholera cases. Another concern is that the two versions of the model are not the same, resulting in sub-optimal parameter estimates for the spatially coupled model, as parameters that maximize the likelihood of the decoupled model almost certainly do not maximize the likelihood of the fully coupled model. These two concerns may explain the unrealistic forecasts and low likelihood of Model 3 of Lee et al. [1] (see Table 2).

At the time Lee et al. [1] conducted their study, there was no known algorithm that could readily be used to maximize the likelihood of an arbitrary meta-population POMP model with coupled spatial dynamics, which justifies the spatial decoupling approximation that was used to calibrate model parameters. For our analysis, we calibrate the parameters of the spatially coupled version of Model 3 using the iterated block particle filter (IBPF) algorithm [39]. This algorithm extends the work of Ning and

Ionides [40], who provided theoretic justification for the version of the algorithm that only estimates unit-specific parameters. The IBPF algorithm enables us to directly estimate the parameters of models describing high-dimensional partially-observed nonlinear dynamic systems via likelihood maximization. The ability to directly estimate parameters of Model 3 is responsible for the large increase in model likelihoods reported in Table 2. Simulations from the fitted model are displayed in Fig. 5.

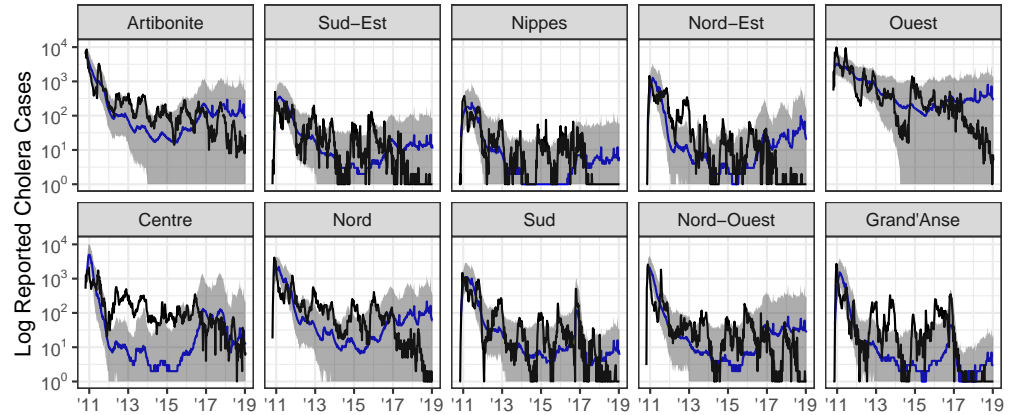


Fig 5. Simulations from Model 3 compared to reported cholera cases. Simulations from initial conditions using the spatially coupled version of Model 3. The black curve represents true case count, the blue line the median of 500 simulations from the model, and the gray ribbons representing 95% confidence interval.

Model Diagnostics

The goal of parameter calibration—whether done using Bayesian or frequentist methods—is to find the best description of the observed data under the assumptions of the model. Obtaining the best fitting set of parameters for a given model does not, however, guarantee that the model provides an accurate representation of the system under investigation. Model misspecification, which may be thought of as the omission of a mechanism in the model that is an important feature of the dynamic system, is inevitable at all levels of model complexity. To make progress, while accepting proper limitations, one must bear in mind the much-quoted observation of George Box [41] that “all models are wrong but some are useful.” Beyond being good practical advice for applied statistics, this assertion is relevant for the philosophical justification of statistical inference as severe testing [42]. In this section, we discuss some tools for diagnosing mechanistic models with the goal of making the subjective assessment of model “usefulness” more objective. To do this, we will rely on the quantitative ability of the model to match the observed data, which we call the model’s *goodness-of-fit*, with the guiding principle that a model which cannot adequately describe observed data may not be reliable for useful purposes. Goodness-of-fit may provide evidence supporting the causal interpretation of one model versus another, but cannot by itself rule out the possibility of alternative explanations.

One common approach to assess a mechanistic model’s goodness-of-fit is to compare simulations from the fitted model to the observed data. Visual inspection may indicate defects in the model, or may suggest that the observed data are a plausible realization of the fitted model. While visual comparisons can be informative, they provide only a weak and informal measure of the goodness-of-fit of a model. The study by Lee et al. [1]

provides an example of this: their models and parameter estimates resulted in simulations that visually resembled the observed data, yet resulted in model likelihoods that were considerably smaller than likelihoods that can be achieved via the likelihood based optimization techniques that were used (see Table 2). Alternative forms of model validation should therefore be used in conjunction with visual comparisons of simulations to observed data.

Another approach is to compare a quantitative measure of the model fit (such as MSE, predictive accuracy, or model likelihood) among all proposed models. These comparisons, which provide insight into how each model performs relative to the others, are quite common [43, 44]. To calibrate relative measures of fit, it is useful to compare against a model that has well-understood statistical ability to fit data, and we call this model a *benchmark*. Standard statistical models, interpreted as associative models without requiring any mechanistic interpretation of their parameters, provide suitable benchmarks. Examples include linear regression, auto regressive moving average time series models, or even independent and identically distributed measurements. Benchmarks enable us to evaluate the goodness of fit that can be expected of a suitable mechanistic model.

Associative models are not constrained to have a causal interpretation, and typically are designed with the sole goal of providing a statistical fit to data. Therefore, we should not require a candidate mechanistic model to beat all benchmarks. However, a mechanistic model which falls far short against benchmarks is evidently failing to explain some substantial aspect of the data. A convenient measure of fit should have interpretable differences that help to operationalize the meaning of far short. Ideally, the measure should also have favorable theoretical properties. Consequently, we focus on log-likelihood as a measure of goodness of fit, and we adjust for the degrees of freedom of the models to be compared by using the Akaike information criterion (AIC) [45].

In some cases, a possible benchmark model could be a generally accepted mechanistic model, but often no such model is available. Because of this, we use a simple negative binomial model with an auto regressive mean as our associative benchmark; this model is described in (35).

$$Y_n|Y_{n-1} \sim \text{NB}(\alpha + \beta Y_{n-1}, \varphi), \quad (35)$$

where $E(Y_n|Y_{n-1}) = \alpha + \beta Y_{n-1}$, and $\text{Var}(Y_n|Y_{n-1}) = E(Y_n|Y_{n-1}) + E(Y_n|Y_{n-1})^2/\varphi$. In the case where the case counts are large, an alternative benchmark recommended by He et al. [16] is a log-linear Gaussian ARMA model; the theory and practice of ARMA models is well developed, and these linear models are appropriate on a log scale due to the exponential growth and decay characteristic of biological dynamics. We chose to use the auto regressive negative binomial model, however, because the large number of weeks with zero recorded cholera cases in department level data makes a benchmark based on a continuous distribution problematic. Likelihoods of Models 1–3 and their respective ARMA benchmark models are provided in Table 2.

It should be universal practice to present measures of goodness of fit for published models, and mechanistic models should be compared against benchmarks. In our literature review of the Haiti cholera epidemic, no non-mechanistic benchmark models were considered in any of the 32 papers that used dynamic models to describe cholera in order to obtain scientific conclusions. Including benchmarks would help authors and readers to detect and confront any major statistical limitations of the proposed mechanistic models. In addition, the published goodness of fit provides a concrete point of comparison for subsequent scientific investigations. When combined with online availability of data and code, objective measures of fit provide a powerful tool to accelerate scientific progress, following the paradigm of the *common task framework* [46].

The use of benchmarks may also be beneficial when developing models at differing

spatial scales, where a direct comparison between model likelihoods is meaningless. In such a case, a benchmark model can be fit to each spatial resolution being considered, and each model compared to their respective benchmark. Large advantages (or shortcomings) in model likelihood relative to the benchmark for a given spatial scale that are not present in other spatial scales may provide weak evidence for (or against) the statistical fit of models across a range of spatial resolutions.

Comparing model log-likelihoods to a suitable benchmark may not be sufficient to identify all the strengths and weaknesses of a given model. Additional techniques include the inspection of conditional log-likelihoods of each observation given the previous observations in order to understand how well the model describes each data point (Sec. S5). Other tools include plotting the effective sample size of each observation [47]; plotting the values of the hidden states from simulations (S5 Text); and comparing summary statistics of the observed data to simulations from the model [34, 48].

Corroborating Fitted Models with Scientific Knowledge

The resulting mechanisms in a fitted model can be compared to current scientific knowledge about a system. Agreement between model based inference and our current understanding of a system may be taken as a confirmation of both model based conclusions and our scientific understanding. On the other hand, comparisons may generate unexpected results that have the potential to spark new scientific knowledge [49].

In the context of our case study, we demonstrate how the fit of Model 1 corroborates other evidence concerning the role of rainfall in cholera epidemics. Specifically, we examine the results of fitting the flexible cubic spline term in Model 1 (Eqs. (3)–(4)). The cubic splines permit flexible estimation of seasonality in the force of infection, $\beta(t)$. Fig. 6 shows that the estimated seasonal transmission rate β mimics the rainfall dynamics in Haiti, despite Model 1 not having access to rainfall data. This is consistent with previous studies finding that rainfall played an important role in cholera transmission in Haiti [50, 51]. The estimated seasonality also features an increased transmission rate during the fall, which was noticed at an earlier stage of the epidemic [43]; the high transmission rate in the fall may also be a result of the increase in transmission that occurred in the fall of 2016, when hurricane Matthew struck Haiti [17].

For any model-based inference, it is important to recognize and assess the modeling simplifications and assumptions that were used in order to arrive at the conclusions. In epidemiological studies, for example, quantitative understanding of individual-level processes may not perfectly match model parameters that were fit to population-level case counts, even when the model provides a strong statistical fit [16]. This makes direct interpretation of estimated parameters delicate.

Our case study provides an example of this in the parameter estimate for the duration of natural immunity due to cholera infection, μ_{RS}^{-1} . Under the framework of Model 2, the best estimate for this parameter is 3.28×10^{12} yr, suggesting that individuals have effectively permanent immunity to cholera once infected. To interpret this result, we bear in mind that the data ranged from 2010–2019, and therefore estimates of immunity longer than 10 yr—the upper end of previous estimates of natural immunity [52]—effectively result in the same model dynamics. The depletion of susceptible individuals may also be attributed to confounding mechanisms—such as localized vaccination programs and non-pharmaceutical interventions that reduce cholera transmission [6, 24]—that were not accounted for in the model. Perhaps the best interpretation of the estimated parameter, then, is that under the modeling framework that was used, the model most adequately describes the observed data by having a steady decrease in the number of susceptible individuals. The weak statistical fit of Model 2 compared to a log-linear benchmark (see Table 2) cautions us against drawing

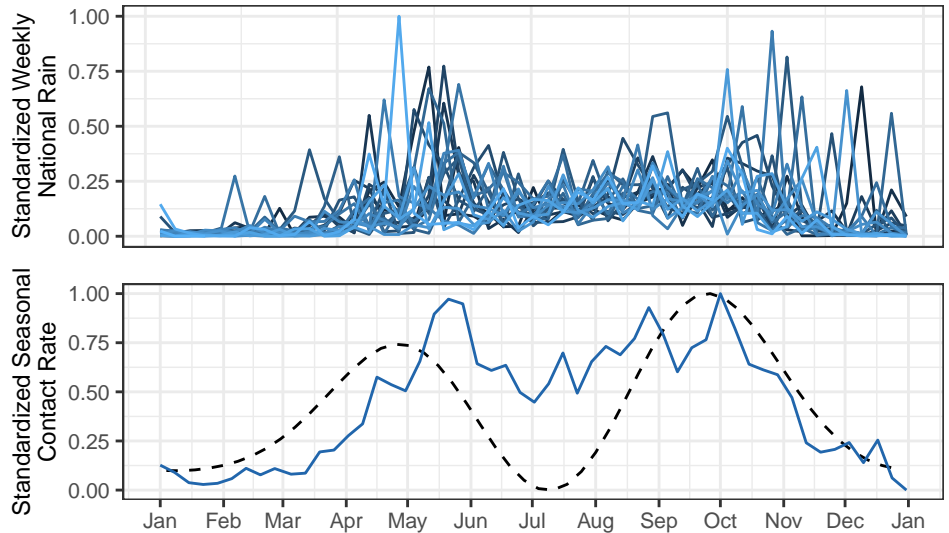


Fig 6. Seasonality of Model 1 transmission compared to rainfall data. (Top) weekly rainfall in Haiti, lighter colors representing more recent years. (Bottom) estimated seasonality in the transmission rate (dashed line) plotted alongside mean rainfall (solid line). The outsized effect of rainfall in the fall may be due to Hurricane Matthew, which struck Haiti in October of 2016 and resulted in an increase of cholera cases in the nation.

quantitative conclusions from this model. A model that has a poor statistical fit may nevertheless provide a useful conceptual framework for thinking about the system under investigation. However, a claim that the model has been validated against data should be reserved for situations where the model provides a statistical fit that is competitive against alternative explanations.

A model which aspires to provide quantitative guidance for assessing interventions should provide a quantitative statistical fit for available data. However, strong statistical fit does not guarantee a correct causal structure: it does not even necessarily require the model to assert a causal explanation. A causal interpretation is strengthened by corroborative evidence. For example, reconstructed latent variables (such as numbers of susceptible and recovered individuals) should make sense in the context of alternative measurements of these variables [53]. In the context of our case study, by reconstructing the latent states of Model 3, we notice that the calibrated model favors higher levels of cholera transmission than what was typically observed in the incidence data (S5 Text). This result hints at the possibility of model misspecification, and should prompt us to be sceptical of the reliability of forecasts from this model. Similarly, parameters that have been calibrated to data should make sense in the context of alternative lines of evidence about the phenomena being modeled, while making allowance for the possibility that the interpretations of parameters may vary when modeling across differing spatial scales.

Results

Forecasts

Forecasts are an attempt to provide an accurate estimate of the future state of a system based on currently available data, together with an assessment of uncertainty. Forecasts from mechanistic models that are compatible with current scientific understanding may

also provide estimates of the future effects of potential interventions. Further, they may enable real-time testing of new scientific hypotheses [54].

Recent information about a dynamic system should be more relevant for a forecast than older information. This assertion may seem self-evident, but it is not the case for deterministic models, for which the initial conditions together with the parameters are sufficient for forecasting, and so recent data do not have special importance. Epidemiological forecasts based on deterministic models are not uncommon in practice, despite their limitations [34]. That may explain why Lee et al. [1] chose to obtain forecasts by simulating the calibrated models forward from initial conditions. We obtain forecasts by simulating future values using latent states that are consistent with the most recent observations; this is done by drawing latent states at the last observation time (t_N) from the filtering distribution $f_{\mathbf{x}_N|\mathbf{y}_{1:N}}(\mathbf{x}_N|\mathbf{y}_{1:N}^*; \hat{\theta})$. The decision not to do this partially explains the unsuccessful forecasts of Lee et al. [1]: their Table S7 shows that the subset of their simulations which were consistent with observing zero cases in 2019 also accurately predicted the prolonged absence of detected cholera.

Uncertainty in just a single parameter can lead to drastically different forecasts [5]. Therefore, parameter uncertainty should also be considered when obtaining model forecasts to influence policy. If a Bayesian technique is used for parameter estimation, a natural way to account for parameter uncertainty is to obtain simulations from the model where each simulation is obtained using parameters drawn from the estimated posterior distribution. For frequentist inference, one possible approach is obtaining model forecasts from various values of θ , where the values of θ are sampled proportionally according to their corresponding likelihoods [34] (S6 Text). Both of these approaches share the similarity that parameters are chosen for the forecast approximately in proportion to their corresponding value of the likelihood function, $f_{\mathbf{y}_{1:N}}(\mathbf{y}_{1:N}^*; \theta)$. In this analysis, we do not construct forecasts accounting for parameter uncertainty as our focus is on the estimation and diagnosis of mechanistic models. Furthermore, we use the projections from a single point estimate to highlight the deficiency of deterministic models that the only variability in model projections is a result of parameter uncertainty, which can lead to over-confidence in forecasts [34].

The primary forecasting goal of Lee et al. [1] was to investigate the potential consequences of vaccination interventions on a system to inform policy. One outcome of their study include estimates for the probability of cholera elimination under several possible vaccination scenarios. Mimicking their approach, we define cholera elimination as an absence of cholera infections for at least 52 consecutive weeks, and we provide forecasts under the following vaccination scenarios:

V0: No additional vaccines are administered.

V1: Vaccination limited to the departments of Centre and Artibonite, deployed over a two-year period.

V2: Vaccination limited to three departments: Artibonite, Centre, and Ouest deployed over a two-year period.

V3: Countrywide vaccination implemented over a five-year period.

V4: Countrywide vaccination implemented over a two-year period.

Simulations from probabilistic models (Models 1 and 3) represent possible trajectories of the dynamic system under the scientific assumptions of the models. Estimates of the probability of cholera elimination can therefore be obtained as the proportion of simulations from these models that result in cholera elimination. The results of these projections are summarized in Figs. 7.

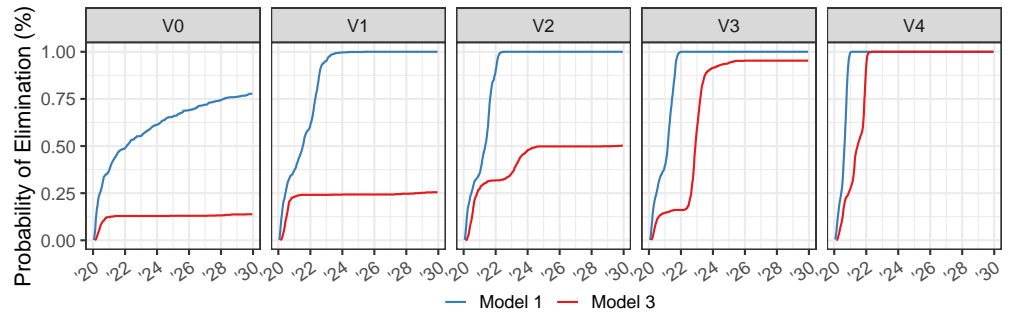


Fig 7. Simulated probability of elimination using Models 1 and 3. Probability of cholera elimination, defined as having zero cholera infectious for at least 52 consecutive weeks, based on 10 year simulations from calibrated versions of Models 1 and 3. Compare to Fig. 3A of Lee et al. [1].

Probability of elimination estimates of this form are not meaningful for deterministic models, as the trajectory of these models only represent the mean behavior of the system rather than individual potential outcomes. We therefore do not provide probability of elimination estimates under Model 2, but show trajectories under the various vaccination scenarios using this model (Fig. 4).

Discussion

The ongoing global COVID-19 pandemic has provided a clear example on how government policy may be affected by the conclusions of scientific models [5]. This article demonstrates that fitting appropriate scientific models to guide policy is a challenging statistical task. In our case study, we found that additional attention to statistical details could have resulted in improved statistical fits to the observed incidence data, leading to improvements in the accuracy of the resulting policy guidance. We used the same data and models, and even much of the same code, as Lee et al. [1], and yet ended up with drastically different conclusions. We acknowledge the benefit of hindsight: our demonstration of a statistically principled route to obtain better-fitting models resulting in more robust insights does not rule out the possibility of discovering other models that fit well yet predict poorly.

Inference for mechanistic time series models offers opportunities for understanding and controlling complex dynamic systems. This case study has investigated issues requiring attention when applying powerful new statistical techniques that can enable statistically efficient inference for a general class of partially observed Markov process models. Researchers should check that the computationally intensive numerical calculations are carried out adequately. Comparison against benchmarks and alternative model specifications should be considered to evaluate the statistical goodness-of-fit. Once that is accomplished, care is required to assess what causal conclusions can properly be inferred given the possibility of alternative explanations consistent with the data. Studies that combine model development with thoughtful data analysis, supported by a high standard of reproducibility, build knowledge about the system under investigation. Cautionary warnings about the difficulties inherent in understanding complex systems [5, 49, 55] should motivate us to follow best practices in data analysis, rather than avoiding the challenge.

Reproducibility and Extendability

Lee et al. [1] published their code and data online, and this reproducibility facilitated our work. Robust data analysis requires not only reproducibility but also extendability: if one wishes to try new model variations, or new approaches to fitting the existing models, or plotting the results in a different way, this should not be excessively burdensome. Scientific results are only trustworthy so far as they can be critically questioned, and an extendable analysis should facilitate such examination [56].

We provide a strong form of reproducibility, as well as extendability, by developing our analysis in the context of a software package, `haitipkg`, written in the R language [57]. Using a software package mechanism supports documentation, standardization and portability that promote extendability. In the terminology of Gentleman and Temple Lang [56], the source code for this article is a *dynamic document* combining code chunks with text. In addition to reproducing the article, the code can be extended to examine alternative analysis to that presented. The dynamic document, together with the R packages, form a *compendium*, defined by Gentleman and Temple Lang [56] as a distributable and executable unit which combines data, text and auxiliary software (the latter meaning code written to run in a general-purpose, portable programming environment, which in this case is R).

Supporting information

S1 Fig. Model 1. Flow chart representation of Model 1.

S2 Fig. Model 2. Flow chart representation of Model 2.

S3 Fig. Model 3. Flow chart representation of Model 3.

S1 Table Notation conversion table. Conversions between the notation used here and the notation of Lee et al. (2020) [1].

S1 Text Model details. In depth description of the Markov chain and differential equation interpretations of compartment flow rates, as well as details on the numeric implementation of these models.

S2 Text Initialization models. Additional details of the initialization model that were used for Models 1–3.

S3 Text Measurement models. Additional details of the measurement model that were used for Models 1–3.

S4 Text Likelihood of Lee et al. models. Details of how the log-likelihood of the Lee et al. models were calculated.

S5 Text Likelihood of Lee et al. models. Additional details on the procedures for fitting and diagnosing Model 3.

S6 Text Accounting for parameter uncertainty A description of a empirical-Bayes approach that can be used to account for parameter uncertainty.

Acknowledgments

This work was supported by National Science Foundation grants DMS-1761603 and DMS-1646108. The authors would like to thank Mercedes Pascual and Betz Halloran for helpful discussions. Laura Matrajt provided additional data for the Model 2 analysis.

s

References

1. Lee EC, Chao DL, Lemaitre JC, Matrajt L, Pasetto D, Perez-Saez J, et al. Achieving Coordinated National Immunity and Cholera Elimination in Haiti Through Vaccination: A Modelling Study. *The Lancet Global Health*. 2020;8(8):e1081–e1089.
2. Tracy M, Cerdá M, Keyes KM. Agent-Based Modeling in Public Health: Current Applications and Future Directions. *Annual Review of Public Health*. 2018;39(1):77–94.
3. Pezzoli L. Global Oral Cholera Vaccine Use, 2013–2018. *Vaccine*. 2020;38:A132–A140.
4. Behrend MR, Basáez MG, Hamley JID, Porco TC, Stolk WA, Walker M, et al. Modelling for Policy: The Five Principles of the Neglected Tropical Diseases Modelling Consortium. *PLoS Neglected Tropical Diseases*. 2020;14(4):1–17.
5. Saltelli A, Bammer G, Bruno I, Charters E, Di Fiore M, Didier E, et al. Five Ways to Ensure that Models Serve Society: a Manifesto. *Nature*. 2020;582:428–484.
6. Trevisin C, Lemaitre JC, Mari L, Pasetto D, Gatto M, Rinaldo A. Epidemicity of Cholera Spread and the Fate of Infection Control Measures. *Journal of the Royal Society Interface*. 2022;19(188):20210844.
7. Rubin DHF, Zingl FG, Leitner DR, Ternier R, Compere V, Marseille S, et al. Reemergence of Cholera in Haiti. *New England Journal of Medicine*. 2022;doi:10.1056/NEJMc2213908.
8. Pan American Health Organization. Cholera Epidemic in Hispaniola 2023 - Situation Report 19; 2023. Available from: <https://www.paho.org/en/documents/cholera-outbreak-hispaniola-2023-situation-report-19>.
9. Francois J. Cholera Remains a Public Health Threat in Haiti. *The Lancet Global Health*. 2020;8(8):e984.
10. Rebaudet S, Gaudart J, Piarroux R. Cholera in Haiti. *The Lancet Global Health*. 2020;8(12):e1468.
11. Henrys JH, Lerebours G, Achille MA, Moise K, Raccurt C. Cholera in Haiti. *The Lancet Global Health*. 2020;8(12):e1469.
12. Lee EC, Ternier R, Lessler J, Azman AS, Ivers LC. Cholera in Haiti—Authors’ Reply. *The Lancet Global Health*. 2020;8(12):e1470–e1471.
13. Lucas RE, et al. Econometric Policy Evaluation: A Critique. In: *Carnegie-Rochester Conference Series on Public Policy*. vol. 1; 1976. p. 19–46.

14. Bretó C, Ionides EL. Compound Markov Counting Processes and their Applications to Modeling Infinitesimally Over-Dispersed Systems. *Stochastic Processes and their Applications*. 2011;121:2571–2591.
15. Stocks T, Britton T, Höhle M. Model Selection and Parameter Estimation for Dynamic Epidemic Models via Iterated Filtering: Application to Rotavirus in Germany. *Biostatistics*. 2020;21(3):400–416.
16. He D, Ionides EL, King AA. Plug-and-Play Inference for Disease Dynamics: Measles in Large and Small Towns as a Case Study. *Journal of the Royal Society Interface*. 2010;7:271–283.
17. Ferreira S. Cholera threatens Haiti after Hurricane Matthew. *BMJ*. 2016;355:i5516.
18. Bretó C, He D, Ionides EL, King AA. Time Series Analysis via Mechanistic Models. *Annals of Applied Statistics*. 2009;3:319–348.
19. Toni T, Welch D, Strelkowa N, Ipsen A, Stumpf MPH. Approximate Bayesian Computation Scheme for Parameter Inference and Model Selection in Dynamical Systems. *Journal of the Royal Society Interface*. 2009;6:187–202.
20. Andrieu C, Doucet A, Holenstein R. Particle Markov chain Monte Carlo methods. *Journal of the Royal Statistical Society, Series B (Statistical Methodology)*. 2010;72:269–342.
21. Ionides EL, Nguyen D, Atchadé Y, Stoev S, King AA. Inference for Dynamic and Latent Variable Models via Iterated, Perturbed Bayes Maps. *Proceedings of the National Academy of Sciences of the USA*. 2015;112(3):719—724.
22. Arulampalam MS, Maskell S, Gordon N, Clapp T. A Tutorial on Particle Filters for Online Nonlinear, Non-Gaussian Bayesian Tracking. *IEEE Transactions on Signal Processing*. 2002;50:174 – 188.
23. Rebaudet S, Bulit G, Gaudart J, Michel E, Gazin P, Evers C, et al. The Case-Area Targeted Rapid Response Strategy to Control Cholera in Haiti: A Four-Year Implementation Study. *PLoS Neglected Tropical Diseases*. 2019;13(4):e0007263.
24. Rebaudet S, Dély P, Boncy J, Henrys JH, Piarroux R. Toward Cholera Elimination, Haiti. *Emerging Infectious Diseases*. 2021;27(11):2932.
25. Ionides EL, Breto C, Park J, Smith RA, King AA. Monte Carlo Profile Confidence Intervals for Dynamic Systems. *Journal of the Royal Society Interface*. 2017;14:1–10.
26. King AA, Nguyen D, Ionides EL. Statistical Inference for Partially Observed Markov Processes via the R Package pomp. *Journal of Statistical Software*. 2016;69:1–43.
27. Kermack WO, McKendrick AG. A Contribution to the Mathematical Theory of Epidemics. *Proceedings of the Royal Society of London, Series A*. 1927;115(772):700–721.
28. Brauer F. *Mathematical Epidemiology: Past, Present, and Future*. *Infectious Disease Modelling*. 2017;2(2):113–127.

29. Giordano G, Blanchini F, Bruno R, Colaneri P, Di Filippo A, Di Matteo A, et al. Modelling the COVID-19 Epidemic and Implementation of Population-Wide Interventions in Italy. *Nature Medicine*. 2020;26(6):855–860.
30. Dadlani A, Afolabi RO, Jung H, Sohraby K, Kim K. Deterministic Models in Epidemiology: From Modeling to Implementation. *arXiv:200404675*. 2020;.
31. Ndi MZ, Supriatna AK. Stochastic Mathematical Models in Epidemiology. *Information*. 2017;20:6185–6196.
32. Asfaw K, Park J, King AA, Ionides EL. Partially Observed Markov Processes with Spatial Structure via the R Package spatPomp. *arXiv:210101157v3*. 2023;.
33. King AA, Rowan T. **subplex**: Unconstrained Optimization using the Subplex Algorithm. R package, available at <https://cranr-project.org/web/packages/subplex>. 2020;.
34. King AA, Domenech de Cellès M, Magpantay FM, Rohani P. Avoidable Errors in the Modelling of Outbreaks of Emerging Pathogens, with Special Reference to Ebola. *Proceedings of the Royal Society B: Biological Sciences*. 2015;282(1806):20150347.
35. Collins OC, Govinder KS. Incorporating Heterogeneity into the Transmission Dynamics of a Waterborne Disease Model. *Journal of Theoretical Biology*. 2014;356:133–143.
36. Green KC, Armstrong JS. Simple Versus Complex Forecasting: The Evidence. *Journal of Business Research*. 2015;68(8):1678–1685.
37. Rebeschini P, van Handel R. Can Local Particle Filters Beat the Curse of Dimensionality? *The Annals of Applied Probability*. 2015;25(5):2809–2866.
38. Park J, Ionides EL. Inference on High-Dimensional Implicit Dynamic Models using a Guided Intermediate Resampling Filter. *Statistics & Computing*. 2020;30:1497–1522.
39. Ionides EL, Ning N, Wheeler J. An Iterated Block Particle Filter for Inference on Coupled Dynamic Systems with Shared and Unit-Specific Parameters. *Statistica Sinica*,. 2022; p. pre-published online.
40. Ning N, Ionides EL. Iterated Block Particle Filter for High-dimensional Parameter Learning: Beating the Curse of Dimensionality. *arXiv:211010745*. 2021;.
41. Box GE. Robustness in the Strategy of Scientific Model Building. In: *Robustness in Statistics*. Elsevier; 1979. p. 201–236.
42. Mayo DG. *Statistical Inference as Severe Testing*. Cambridge: Cambridge University Press; 2018.
43. Rinaldo A, Bertuzzo E, Mari L, Righetto L, Blokesch M, Gatto M, et al. Reassessment of the 2010-2011 Haiti Cholera Outbreak and Rainfall-Driven Multiseason Projections. *Proceedings of the National Academy of Sciences*. 2012;109(17):6602–6607.
44. Sallah K, Giorgi R, Bengtsson L, Lu X, Wetter E, Adrien P, et al. Mathematical Models for Predicting Human Mobility in the Context of Infectious Disease Spread: Introducing the Impedance Model. *International Journal of Health Geographics*. 2017;16(1):1–11.

45. Akaike H. A New Look at the Statistical Model Identification. *IEEE Transactions on Automatic Control*. 1974;19(6):716–723.
46. Donoho D. 50 Years of Data Science. *Journal of Computational and Graphical Statistics*. 2017;26(4):745–766.
47. Liu JS. *Monte Carlo Strategies in Scientific Computing*. New York: Springer; 2001.
48. Wood SN. Statistical Inference for Noisy Nonlinear Ecological Dynamic Systems. *Nature*. 2010;466:1102–1104.
49. Ganusov VV. Strong Inference in Mathematical Modeling: a Method for Robust Science in the Twenty-First Century. *Frontiers in Microbiology*. 2016;7:1131.
50. Lemaitre J, Pasetto D, Perez-Saez J, Sciarra C, Wamala JF, Rinaldo A. Rainfall as a Driver of Epidemic Cholera: Comparative Model Assessments of the Effect of Intra-Seasonal Precipitation Events. *Acta Tropica*. 2019;190:235–243.
51. Eisenberg MC, Kujbida G, Tuite AR, Fisman DN, Tien JH. Examining Rainfall and Cholera Dynamics in Haiti using Statistical and Dynamic Modeling Approaches. *Epidemics*. 2013;5(4):197–207.
52. King AA, Ionides EL, Pascual M, Bouma MJ. Inapparent Infections and Cholera Dynamics. *Nature*. 2008;454:877–880.
53. Grad YH, Miller JC, Lipsitch M. Cholera Modeling: Challenges to Quantitative Analysis and Predicting the Impact of Interventions. *Epidemiology*. 2012;23(4):523.
54. Lewis ASL, Rollinson CR, Allyn AJ, Ashander J, Brodie S, Brookson CB, et al. The Power of Forecasts to Advance Ecological Theory. *Methods in Ecology and Evolution*,. 2022; p. pre-published online.
55. Ioannidis JP, Cripps S, Tanner MA. Forecasting for COVID-19 has Failed. *International Journal of Forecasting*. 2020;.
56. Gentleman R, Temple Lang D. Statistical Analyses and Reproducible Research. *Journal of Computational and Graphical Statistics*. 2007;16(1):1–23.
57. R Core Team. *R: A Language and Environment for Statistical Computing*; 2022. Available from: <https://www.R-project.org/>.

Supplement to “Informing policy via dynamic models: Cholera in Haiti”

Jesse Wheeler, AnnaElaine L. Rosengart, Zhuoxun Jiang,
Kevin Tan, Noah Treutle and Edward L. Ionides

Department of Statistics, University of Michigan

October 6, 2023

Supplementary Content

S1 Model Diagrams	2
S2 Markov chain and differential equation interpretations of compartment flow rates	4
S3 Numerical solutions to compartment models	6
S4 Measurement Models	7
S5 Initial Values	9
S6 Calibrating Model 3 to observed cases	10
S7 Replication of Lee et al. (2020a)	16
S8 Forecasting with parameter uncertainty	22
S9 Translating to Lee et al. (2020a) notation	23

S1 Model Diagrams

Each of the dynamic models considered in this manuscript can be fully described using the model descriptions in the manuscript, coupled with the additional information described in Sections 2 and 3 of this supplement. Despite this, diagrams of dynamic systems are often helpful to understand the equations. In this section, we give three diagrams representing Models 1–3, respectively. Because the models are defined by their mathematical equations and numeric implementation, these diagrams are not unique visual representations of the model. Alternative representations that may be helpful in understanding the models explored in this paper were made by Lee et al. (2020b).

S1.1 Model 1

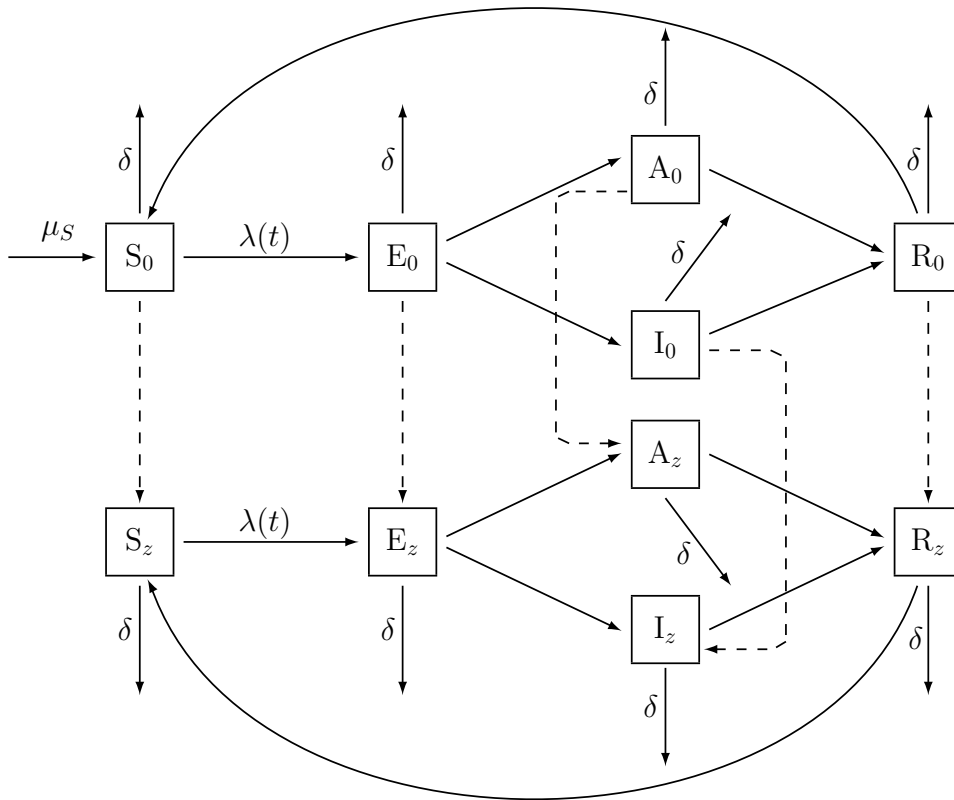


Fig S-1: A flow diagram for the SEAIR model.

S1.2 Model 2

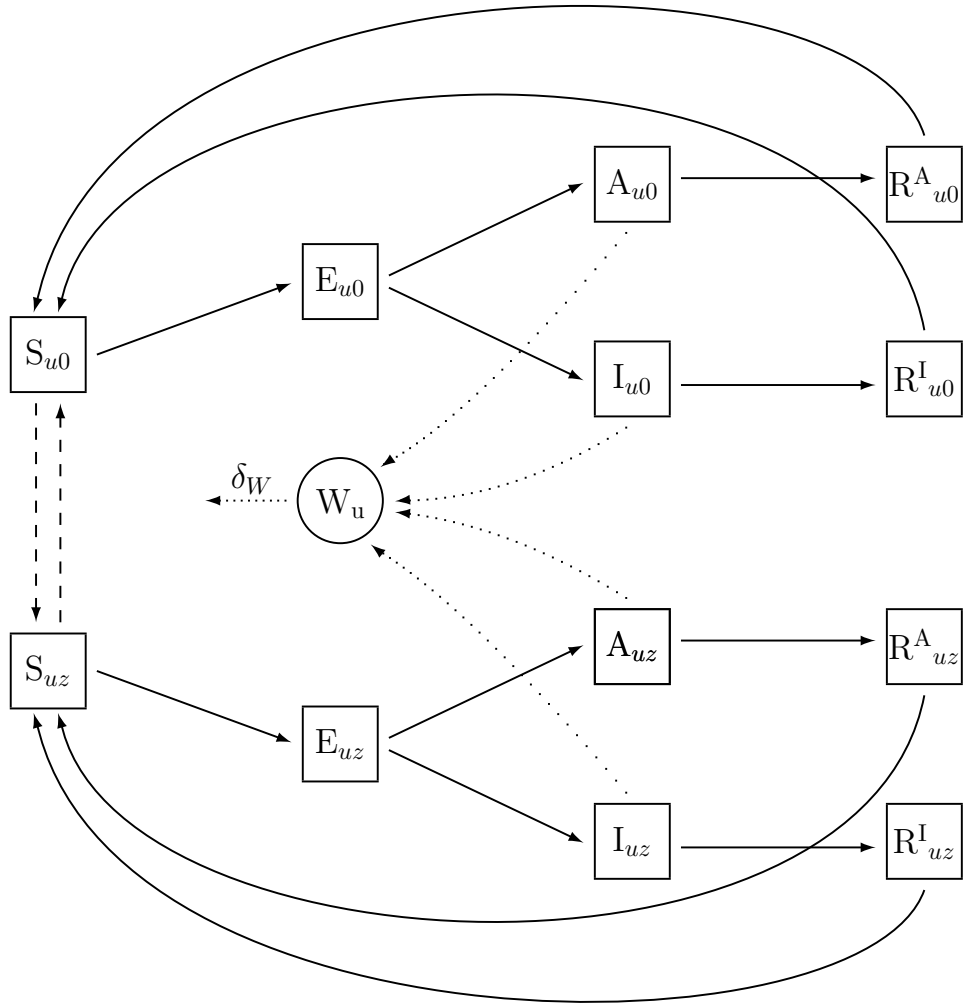


Fig S-2: A flow diagram for the SEAIR model 2. This is a constant population model, there are no births/deaths. Vaccinations are assumed to only be given to susceptible individuals, and vaccine immunity wanes only with susceptible vaccinated individuals.

S1.3 Model 3

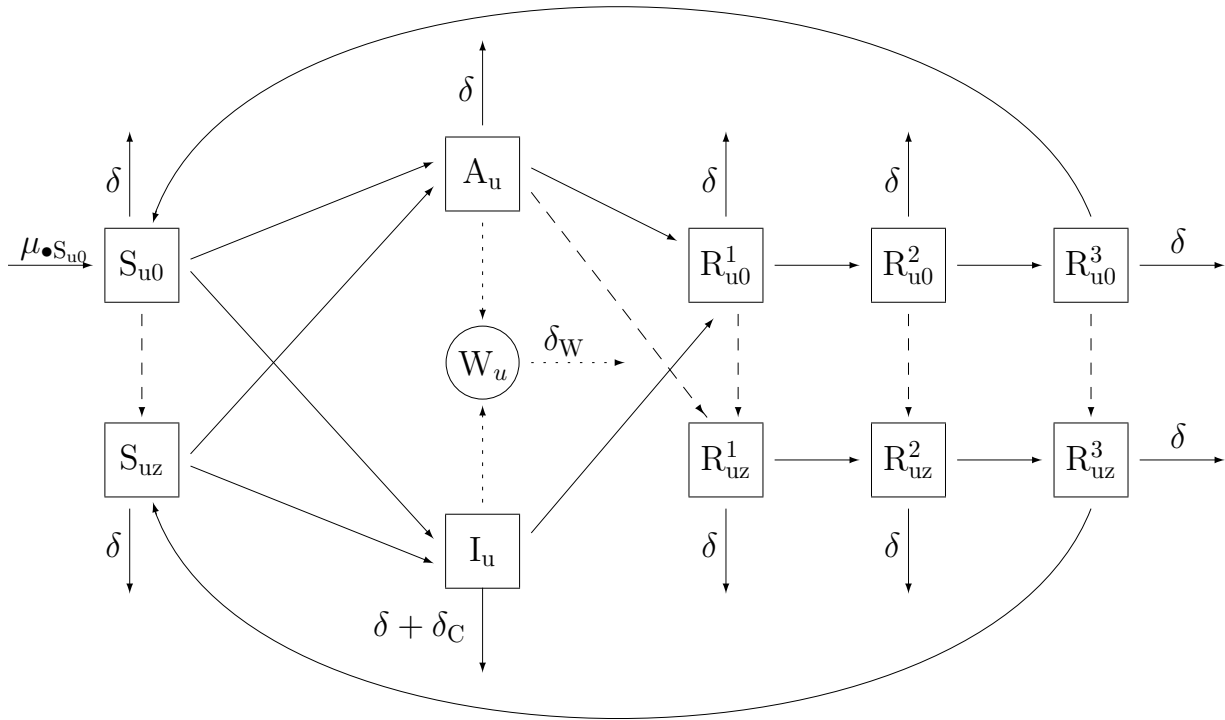


Fig S-3: A flow diagram for the SAIR model 3. This model assumes a constant population while also including a mechanism for births/deaths; all deaths are balanced by births into the unvaccinated susceptible compartment, so the birth rate $\mu_{\bullet S_{u0}}$ corresponds to the sum total deaths from the remaining compartments. The model assumes that symptomatic individuals will not be vaccinated, hence no vaccination arrow exiting the I_{u0} compartment.

S2 Markov chain and differential equation interpretations of compartment flow rates

In Sections 2.1, 2.2 and 2.3 of the main article, we define compartment models in terms of their flow rates. For a discrete population model, these rates define a Markov chain. For a continuous

and deterministic model, the rates define a system of ordinary differential equations. Here, we add additional details to clarify the mapping from a collection of rate functions to a fully specified process. Our treatment follows Bretó et al. (2009).

A general compartment model is a vector-valued process $X(t) = (X_1(t), \dots, X_c(t))$ denoting the (integer or real-valued) counts in each of c compartments, where t is any continuous value in the interval $[t_0, \infty)$ for some real valued starting time t_0 . The compartments may also have names, but to set up general notation we simply refer to them by their numerical index. The basic characteristic of a compartment model is that $X(t)$ can be written in terms of the flows $N_{ij}(t)$ from i to j . A flow into compartment i from outside the system is denoted by $N_{\bullet i}$, and a flow out of the system from compartment i is denoted by $N_{i\bullet}$. We call \bullet a source/sink compartment, though it is an irregular compartment since $X_{\bullet}(t)$ is not defined. These flows are required to satisfy a “conservation of mass” identity:

$$X_i(t) = X_i(t_0) + N_{\bullet i}(t) - N_{i\bullet}(t) + \sum_{j \neq i} N_{ji}(t) - \sum_{j \neq i} N_{ij}(t). \quad (\text{S1})$$

Each flow $N_{ij}(t)$ is associated with a rate function $\mu_{ij} = \mu_{ij}(t, X(t))$, where we include the possibility that i or j takes value \bullet .

There are different ways to use a collection of rate functions to build a fully specified model. We proceed to describe the ones we use in this paper: via a system of ordinary differential equations (Sec. S2.1), a simple Markov counting system (Sec. S2.2), and an overdispersed Markov counting system (Sec. S2.3). Other representations include stochastic differential equations driven by Gaussian noise or Gamma noise (Bhadra et al., 2011).

S2.1 Ordinary differential equation (ODE) interpretation

A basic deterministic specification is

$$dN_{ij}/dt = \mu_{ij}(t, X(t))X_i(t), \quad i \in 1:c, \quad j \in 1:c \cup \{\bullet\}, \quad i \neq j, \quad (\text{S2})$$

where $\mu_{ij}(t, X(t))$ is called a per-capita rate or a unit rate. Flows into the system require special treatment since $X_i(t)$ in (S2) is not defined for $i = \bullet$. Instead, we specify

$$dN_{\bullet i}/dt = \mu_{\bullet i}(t, X(t)). \quad (\text{S3})$$

This is the the interpretation and implementation used for Model 2 in our study.

S2.2 Simple Markov counting system interpretation

A continuous time Markov chain can be specified via its infinitesimal transition probabilities. A basic approach to this is to define

$$\mathbb{P}[N_{ij}(t + \delta) - N_{ij}(t) = 0 \mid X(t)] = 1 - \delta\mu_{ij}(t, X(t))X_i(t) + o(\delta), \quad (\text{S4})$$

$$\mathbb{P}[N_{ij}(t + \delta) - N_{ij}(t) = 1 \mid X(t)] = \delta\mu_{ij}(t, X(t))X_i(t) + o(\delta), \quad (\text{S5})$$

for $i \in 1:c$ and $j \in 1:c \cup \{\bullet\}$ with $i \neq j$. As with the ODE case, we need special attention for flows into the system, and we define

$$\mathbb{P}[N_{\bullet i}(t + \delta) - N_{\bullet i}(t) = 0 \mid X(t)] = 1 - \delta\mu_{\bullet i}(t, X(t)) + o(\delta), \quad (\text{S6})$$

$$\mathbb{P}[N_{\bullet i}(t + \delta) - N_{\bullet i}(t) = 1 \mid X(t)] = \delta\mu_{\bullet i}(t, X(t)) + o(\delta). \quad (\text{S7})$$

Together with the initial conditions $X(0)$, equations (S4)–(S7) define a Markov chain. Each flow is a simple counting process, meaning a non-decreasing integer-valued process that only has jumps of size one. We therefore call the Markov chain a simple Markov counting system (SMCS). The infinitesimal mean of every flow is equal to its infinitesimal variance (Bretó and Ionides, 2011) and so an SMCS is called equidispersed. We note that the special case of Model 1 used by Lee et al. (2020a) (with $\sigma_{\text{proc}} = 0$) is an SMCS. To permit more general mean-variance relationships for a Markov counting system, we must permit jumps of size greater than one. The utility of overdispersed models, where the infinitesimal variance of the flow exceeds the infinitesimal mean, has become widely recognized (Stocks et al., 2020; He et al., 2010).

S2.3 Overdispersed Markov counting system interpretation

Including white noise in the rate function enables the possibility of an overdispersed Markov counting system (Bretó and Ionides, 2011; Bretó et al., 2009; He et al., 2010). Since rates should be non-negative, Gaussian noise is not appropriate and gamma noise is a convenient option that has found various applications (Romero-Severson et al., 2015; Subramanian et al., 2020). Specifically, we consider a model given by

$$\mu_{ij}(t, X(t)) = \bar{\mu}_{ij}(t, X(t)) d\Gamma_{ij}(t)/dt, \quad (\text{S8})$$

where $\Gamma_{ij}(t)$ is a stochastic process having independent gamma distributed increments, with

$$\mathbb{E}[\Gamma_{ij}(t)] = t, \quad \text{Var}[\Gamma_{ij}(t)] = \sigma_{ij}^2 t. \quad (\text{S9})$$

Formally interpreting the meaning of (S8) is not trivial, and we do so by constructing a Markov process $X(t)$ as the limit of the Euler scheme described in Section S3, below. Therefore, the numerical scheme in Sec. S3 can be taken as a definition of the meaning of (S8). The Markov chain defined by the limit of this Euler scheme as the step size decreases is an overdispersed Markov counting system, with the possibility of instantaneous jumps of size greater than one (Bretó and Ionides, 2011).

S3 Numerical solutions to compartment models

Models may be fitted and their implications assessed via numerical solutions (i.e., simulations) from the model equations. All the analyses we consider have this simulation-based property, known as plug-and-play or equation-free or likelihood-free. The numerical solutions to the model are arguably of more direct scientific interest than the exact solutions to the postulated equations. For ODE models, numerical methods are well studied and a standard numerical solution package such as `deSolve` in R is adequate for many purposes. For SMCS and ODMCS models, exact schemes are feasible when the number of events is small, which may be the case for small populations. However, for applicability to larger populations, we use instead the following Euler scheme. Write δ for an Euler time step, and ΔN_{ij} for the numerical approximation to $N_{ij}(t + \delta) - N_{ij}(t)$ given $X(t)$. For each i and j in $1:c \cup \{\bullet\}$ with $i \neq j$, we draw independent Gamma distributed noise increments with mean δ and variance $\sigma_{ij}^2 \delta$, denoted using a mean-variance parameterization of the gamma distribution as

$$\Delta\Gamma_{ij} \sim \text{gamma}(\delta, \sigma_{ij}^2 \delta). \quad (\text{S10})$$

In the case of an SMCS model, $\sigma_{ij} = 0$ for all i and j , so we have $\Delta\Gamma_{ij} = \delta$. Then, for $i \neq \bullet$ and $j \neq i$, and writing

$$\mu_{ij} = \bar{\mu}_{ij}(t, X(t))\Delta\Gamma_{ij}/\delta, \quad (\text{S11})$$

we calculate transition probabilities

$$p_{ij} = \exp \left\{ - \sum_{k \in 1:c \cup \{\bullet\}} \mu_{ik} \delta \right\} \frac{\mu_{ij}}{\sum_{k \in 1:c \cup \{\bullet\}} \mu_{ik}}, \quad (\text{S12})$$

$$p_{ii} = 1 - \sum_{j \neq i} p_{ij}. \quad (\text{S13})$$

These probabilities correspond to competing hazards for every individual in compartment i to transition to some compartment j , interpreting $j = i$ to mean that the individual remains in i . Then, $(\Delta N_{i1}, \dots, \Delta N_{ic}, \Delta N_{i\bullet})$ has the multinomial distribution where $X_i(t)$ individuals are allocated independently to $1 : c \cup \{\bullet\}$ with probabilities given by (S12) and (S13). We use the `reulermultinom` function in the `pomp` package to draw from this multinomial distribution.

Different treatments of demographic flows—such as birth, death, immigration and emigration—are possible. For the case $i = \bullet$, the treatment used by Model 1 is to set

$$\Delta N_{\bullet j} \sim \text{poisson}(\mu_{\bullet j} \delta), \quad (\text{S14})$$

an independent Poisson random variable with mean $\mu_{\bullet j} \delta$.

Models 2 and 3 used an alternative approach, balancing the total number of flows in and out of the compartment, i.e., $\sum_i N_{\bullet i}(t) = \sum_i N_{i\bullet}(t)$, in order to make the model consistent with the known total population. In this case, we formally model the death rate as a rate of returning to the susceptible class S , and use external transitions from \bullet into S to describe only net population increase.

S4 Measurement Models

Each POMP requires specification of a measurement model, which is a statistical description of how observations on the system are obtained. In general, we used the same measurement models that were reported by Lee et al. (2020a) unless specifically noted in the following subsections.

S4.1 Model 1

In this model, the advantage afforded by vaccination is an increased probability that an infection is asymptomatic. Therefore, under the assumptions of this model, all reported cases are assumed to be a fraction of individuals that transition from the exposed to the infected compartment, as noted in Eq. (S15):

$$Y_n \mid \Delta N_{E.I.}(n) = \delta \sim \text{NB}(\rho\delta, \psi), \quad (\text{S15})$$

where Y_n is the reported cholera cases at time $t_n \in t_1 : t_N$ and $\Delta N_{E.I.}(n)$ is the sum total of individuals across each vaccination compartment $z \in 1 : Z$ who moved from compartment E_z to I_z since observation t_{n-1} . Here, $\text{NB}(\rho\delta, \psi)$ denotes a negative binomial distribution with mean $\rho\delta$ and variance $\rho\delta(1 + \frac{\rho\delta}{\psi})$.

S4.2 Model 2

Model 2 was fit using reported case counts that were transformed using the natural logarithm. We fit Model 2 using the subplex algorithm in the `subplex` package, using a Gaussian measurement model (Eq. (S16)) on the log transformed cases within each unit. The final loss function that is maximized is the product of the likelihoods of the individual units, or the sum of the log-likelihood of the individual units. The measurement model for individual units is given in Eq. (S16).

$$\log(Y_{u,n} + 1) \mid \Delta N_{E_u.I_u.}(n) = \delta_u \sim N(\log(\rho\delta_u + 1), \psi^2), \quad (\text{S16})$$

where $\Delta N_{E_u.I_u.}(n)$ is the sum total of individuals across vaccination compartment $z \in 0 : 4$ within unit u who moved from compartment E_{uz} to I_{uz} since observation t_{n-1} . Therefore, because the natural logarithm of observed case counts (plus one, to avoid taking the logarithm of zero) has a normal distribution, $Y_{u,n} + 1$ is assumed to follow a log-normal distribution with log-mean parameter $\log(\rho\Delta N_{E_u.I_u.}(n) + 1)$ and log-variance ψ^2 . We note that fitting a model with this measurement model is equivalent to fitting using least squares, with $\log(Y_{u,n} + 1)$ as the response variable.

This measurement model differs from that used by Lee et al. (2020a), who fit the model in two stages: epidemic and endemic phases. Although their text and supplement material do not explicitly describe the measurement model used, inspection of the code provided with their submission suggests a change in measurement model between the epidemic and endemic phases. The measurement model they used for the epidemic phase is

$$Y_{u,n} \mid \Delta N_{E_u.I_u.}(n) = \delta_u \sim N(\rho\delta_u, \psi^2), \quad (\text{S17})$$

The measurement model they used for the endemic phase modifies the epidemic model by counting both asymptotically infected (A) and symptomatically infected (I) individuals in the case counts:

$$Y_{u,n} \mid \Delta N_{E_u.I_u.}(n) = \delta_{u1}, \Delta N_{E_u.A_u.}(n) = \delta_{u2} \sim N(\rho(\delta_{u1} + \delta_{u2}), \psi^2), \quad (\text{S18})$$

where the notation for $\Delta N_{E_u.A_u.}(n)$ is similar to $\Delta N_{E_u.I_u.}(n)$, described above.

S4.3 Model 3

In this model, reported cholera cases are assumed to stem from individuals who develop symptoms and seek healthcare. Therefore reported cases are assumed to come from an over-dispersed negative binomial model, given the increase in infected individuals:

$$Y_{u,n} \mid \Delta N_{S_u.I_u.}(t) = \delta_u \sim \text{NB}(\rho\delta_u, \psi), \quad (\text{S19})$$

where $\Delta N_{S_u.I_u.}(n)$ is the number of individuals who moved from compartment S_{uz} to I_u since observation t_{n-1} .

This measurement model is a minor change from that used by Lee et al. (2020a), which allowed for a change in the reporting rate on January 1st, 2018. The fitted values of the reporting rate—before and after January 2018—were 0.97 and 0.097, respectively. An instantaneous change from near perfect to almost non-existent reporting can be problematic, as it forces the model to explain the observed reduction in reported cases as a decrease in the reporting of cases, rather than a decrease in the prevalence of cholera. This shift was justified by a “change of the case definition that occurred on January 1st, 2018”; this claim was not cited, and we could find no evidence that such a drastic change in the reporting rate would be warranted. We therefore do not allow a change in reporting rate when fitting Model 3.

S5 Initial Values

To perform inference on POMP models, it is necessary to propose an initial probability density for the latent process $f_{X_0}(x_0; \theta)$, including the possibility that the initial values of the latent states are known, or are a non-random function of the unknown parameter vector, θ . This density is used to obtain initial values of the latent state when fitting and evaluating the model. For each of the models considered in this analysis, the initial conditions are derived by enforcing the model dynamics on reported cholera cases. It is also sometimes necessary to fit some initial value parameters in order to help determine initial values for weakly identifiable compartments. In the following subsections, we mention initial value parameters that were fit for each model.

S5.1 Model 1

For this model, the number of individuals in the Recovered and Asymptomatic compartments are set to zero, but the initial proportion of Infected and Exposed individuals is estimated as initial value parameters ($I_{0,0}$ and $E_{0,0}$, respectively) using the IF2 algorithm, implemented as `mif2` in the `pomp` package. Finally, the initial proportion of Susceptible individuals $S_{0,0}$ is calculated as $S_{0,0} = 1 - I_{0,0} - E_{0,0}$. This model for the initial values of the latent states matches that which was used by Lee et al. (2020a).

S5.2 Model 2

Model 2 assumes that the initial values are a deterministic function of the reporting rate and the initial case reports, and so no initial value parameters need to be estimated. Initial values for latent state compartments are chosen so as to enforce the model dynamics on the observed number of cases. Specifically, the model sets $I_{u0}(0) = y_{1u}^*/\rho$ for each unit $u \in 1 : 10$, where $I_{u0}(t)$ is the number of infected individuals in unit u at time t , vaccination scenario $z = 0$, y_{tu}^* is the reported number of cases, and ρ is the reporting rate. This model for the initial values of the latent states matches that which was used by Lee et al. (2020a).

S5.3 Model 3

The latent states of this model are initialized by enforcing the model dynamics on the incidence data from the start of the recorded cases until time t_0 , requiring that some of the available data be used to determine the initial values of the latent states. This is the same approach that was taken by Lee et al. (2020a), who used the value $t_0 = 2014-02-22$; this choice of t_0 results in modeling roughly only 60% of the available data, some of which is later discarded for alternative reasons (Lee et al., 2020b).

We do not see any immediate reason that this model could not be extended to cover a larger range of the data, and chose the value $t_0 = 2010-11-13$. This choice of t_0 corresponds to using approximately 1% of the available data to determine initial values of the latent states. In addition to modeling a larger portion of the available data, this choice of t_0 corresponds to an important real-world event, as daily reports from each of the departments were not being sent to the health ministry until November 10, 2010 (Barzilay et al., 2013); this choice of t_0 therefore makes $\mathbf{Y}(t_1)$ the first week of data once daily reports are being sent to the health ministry. The few observation times that exist before t_0 are used to initialize the model by enforcing model dynamics on these preliminary observations. For convenience, we denote these observations as t_{-3}, t_{-2} and t_{-1} ; as

before, we let $y_{u,-k} = Y_u(t_{-k})$ denote the observed case count for unit u at time point t_{-k} , where $k \in 1 : 3$. Equations for the initial values of non-zero latent states are provided in Eqs. (S20)–(S24); these equations match those that were used by Lee et al. (2020a), the primary change being a change to the value of t_0 .

$$I_u(t_0) = \frac{y_{u,-1}^*}{7\rho(\mu_{IR} + (\delta + \delta_C)/365)}, \quad (\text{S20})$$

$$A_u(t_0) = \frac{I_{u0}(t_0)(1-f)}{f}, \quad (\text{S21})$$

$$R_{u01}(t_0) = R_{u02}(t_0) = R_{u03}(t_0) = \left(\frac{\sum_{k=-3}^0 y_{u,k}^*}{\rho f} - (I_{u0}(t_0) + A_{u0}(t_0)) \right) / 3 \quad (\text{S22})$$

$$S_{u0}(t_0) = \text{Pop}_u - I_u(t_0) - A_u(t_0) - \sum_{k=1}^3 R_{u0k}(t_0) \quad (\text{S23})$$

$$B_u(t_0) = [1 + a\tilde{J}^r] \text{Den}_u \mu_W [I_u(t_0) + \epsilon_W A_{u0}(t)] / \mu_W. \quad (\text{S24})$$

In Eq. (S24), $\tilde{J} = 0.002376$ is the median adjusted rainfall over the observation period. One important consideration to make with this parameter initialization model is when $y_{u,-1}^* = 0$, which occurs for units $u \in \{3, 4\}$, which correspond to the Grand’Anse and Nippes departments, respectively. When this is the case, each of the infectious $I_u(t_0)$, asymptomatic $A_u(t_0)$, and bacterial reservoir $W_u(t_0)$ compartments have a value of zero. Because Model 3 models cholera transmission primarily by means of the bacterial reservoir, this makes it nearly impossible for an outbreak to occur. Therefore for units $u \in \{3, 4\}$, we introduce initial value parameters $I_{0,0}^3$ and $I_{0,0}^4$, and calibrate these parameter values using the data. The resulting parameter estimates are used to obtain the remaining non-zero initial values of the latent states using Eqs. (S21)–(S24).

S6 Calibrating Model 3 to observed cases

In this section, we provide more detail on the process that was used to estimate the coefficients of Model 3. In particular, we discuss why we decided to include additional model parameters—those that are associated with the behavior of the system during Hurricane Matthew—that were not considered by Lee et al. (2020a). To calibrate this model, we used the iterated block particle filter (IBPF) method of Ionides et al. (2022). Due to the novelty of this algorithm, there does not exist published examples the IBPF algorithm used for data analysis outside of the papers in which the algorithm was introduced (Ning and Ionides, 2021; Ionides et al., 2022), which is one motivation of the inclusion additional details related to fitting and diagnosing the model fit provided here.

Lee et al. (2020a) were only able to estimate model parameters to a simplified version of Model 3 on a subset of the available data, as no method existed at the time of their publication to fit a fully coupled meta-population model to disease incidence data. Building on their results, we fit the fully coupled version of Model 3 to nearly all available data, reserving only a few observations to use to calibrate the initial conditions of the model (see the previous section for more details). In order to properly maximize the model likelihood, we found that it was necessary to use multiple searches for the MLE, periodically pruning away less successful searches. The first collection of searches was performed by obtaining initial values for the parameters by uniformly sampling values from

a predefined hypercube. A subsequent refinement search used parameter values corresponding to the largest model likelihoods as starting parameter values. The need for multiple searches does not appear to be uncommon, as a similar approach was used by Ionides et al. (2022).

We use the technique described above to fit the fully coupled version of Model 3 proposed by Lee et al. (2020a). The maximum likelihood we obtained after two rounds of searching was -17543 , which is higher than the benchmark model (-17933). While beating a simple associative benchmark is promising, this does not immediately rule out the possibility that the model is a poor description of the system. Additional investigation of parameters estimates and their corresponding implications on model based conclusions should always be conducted. For meta-population models, it is worth considering how well the model fits the data to each spatial unit. The likelihoods for each department, compared to the corresponding benchmark model, are displayed in Fig. S-4. The figure demonstrates that while the log-likelihood of the fitted model outperforms the auto-regressive negative binomial benchmark model, Model 3 has lower likelihoods than the benchmark for some departments.

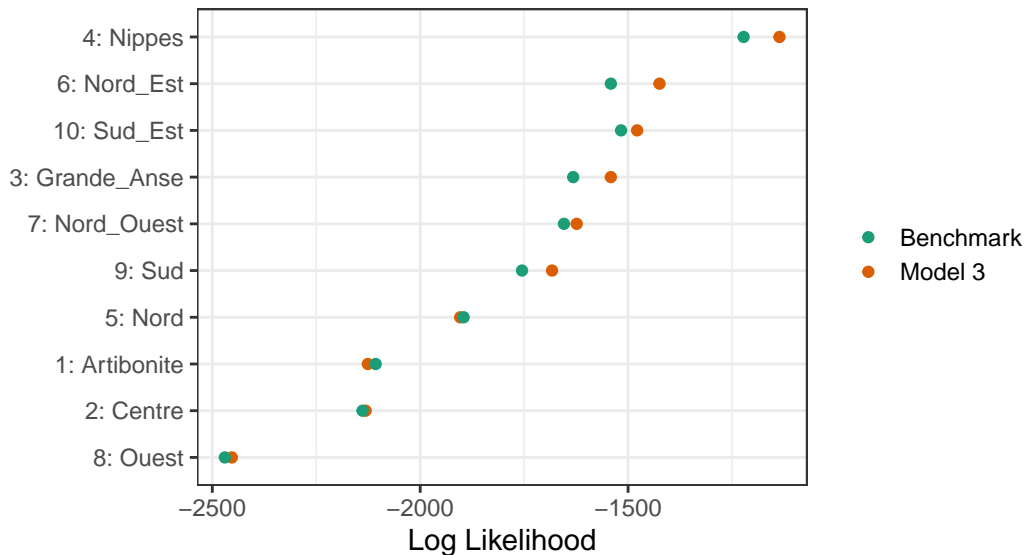


Fig S-4: Log-likelihoods of Model 3 for each department compared to the corresponding benchmark model prior to the inclusion of parameters that account for Hurricane Matthew.

In addition to considering the conditional log-likelihoods of each unit, one can consider conditional log-likelihoods of each observation. When compared to a benchmark, this level of detail can provide useful information about which observations are well described by the model and which are not. In Fig. S-5, we plot the conditional log-likelihoods of Model 3 for each observation. Typically it is most useful to compare the conditional log-likelihoods of the model under consideration to a benchmark, as plotting only conditional log-likelihoods without a comparison may not be helpful. In this case, however, the same insight can be drawn using a figure without a benchmark comparison, so we do not include the benchmark in order to avoid the issue of over-plotting.

Fig. S-5 reveals that the fitted model poorly describes certain features of the data. For example, many departments (in particular Sud) have observations with lower conditional log-likelihoods near October 2016 than at other time points. Further investigation of the model output reveals that the

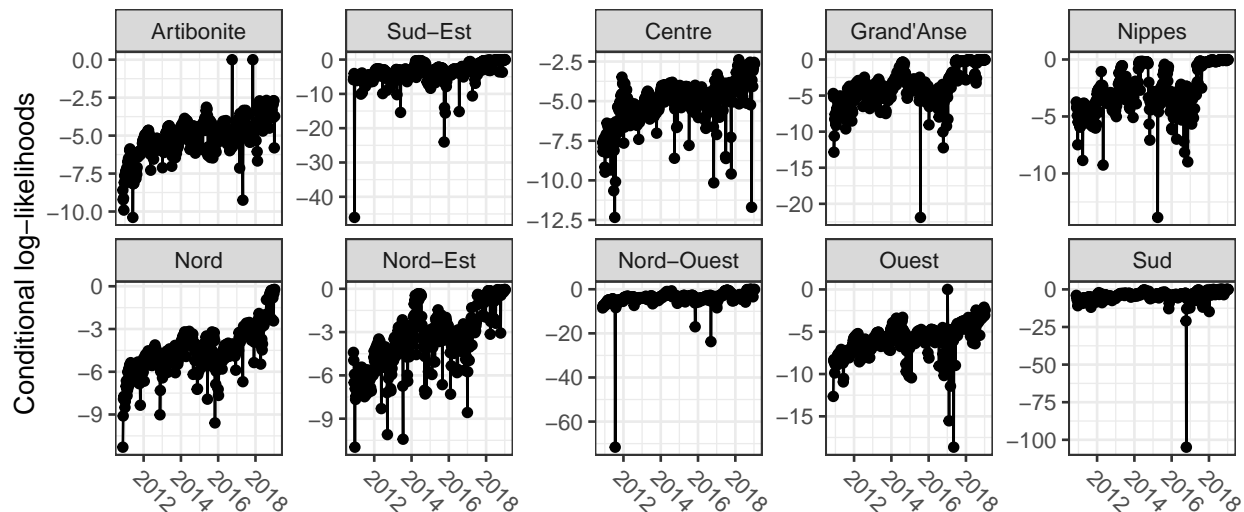


Fig S-5: Conditional log-likelihoods of Model 3 prior to the inclusion of the Hurricane Matthew related parameters.

model is struggling to explain the sudden surge in cholera cases that occurred at this time, which coincides with the time that Hurricane Matthew struck Haiti. While the model does include a mechanism to account for increased cholera transmission due to large rainfall events, the mechanism does not appear to be sufficient to capture the damaging effects of the hurricane, which had the greatest impact in the the Sud and Grand'Anse departments (Ferreira, 2016). This result led us to include parameters $\beta_{W_u}^{hm}$ and h_u^{hm} in Eq. 23 of the main text, which allows for an increase in the transmission rate between environmental cholera and humans for in Sud and Grand'Anse during and after the hurricane. The effect of the hurricane on cholera transmission is assumed to have an exponential decay, where the magnitude is determined by $\beta_{W_u}^{hm}$ and the duration of the effect determined by h_u^{hm} .

We refit Model 3 after introducing these hurricane-related parameters using the same successive search scheme described above. The resulting model has a log-likelihood value of -17402.4 . The addition of the Hurricane parameters seems to have resulted in a dramatic increase in conditional likelihoods around and after October 2016, as seen in Fig. S-6. The inclusion of these parameters resulted in an overall increase of 140.1 log-likelihood units. Such a large difference in log-likelihoods is well beyond the threshold of statistical uncertainty determined by Wilks' theorem, suggesting that the data highly favor the inclusion of the additional parameters.

Now that the model with additional parameters has been calibrated to the incidence data, we plot the conditional log-likelihood of each department compared to a benchmark model in Fig. S-7. Interestingly, the difference in log-likelihoods between Model 3 and the benchmark model is smallest in the departments Artibonite, Nord, Centre and Ouest. Each of these departments also exhibited the most sustained cholera transmission, defined by having the fewest number of weeks with no recorded cholera cases. Specifically, these four departments have zero cholera cases recorded in less than 4% of the available data, and all remaining departments—except for Nord-Ouest, which has approximately 9.5% of cases that are zeros and also exhibits the next smallest difference in log-likelihoods—have zero cases recorded in at least 14% of the available weekly data. This result

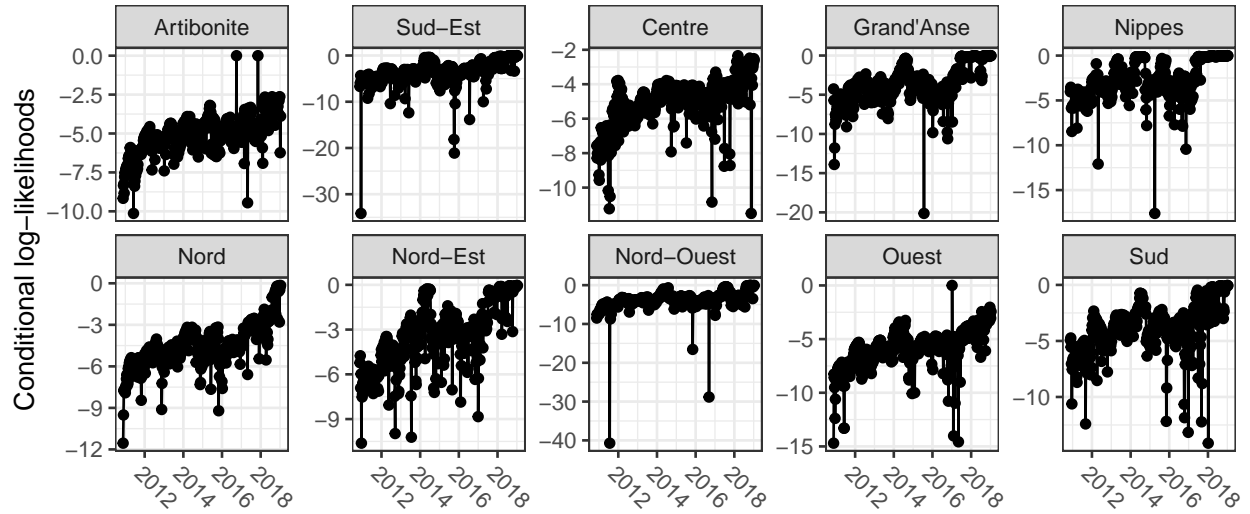


Fig S-6: Conditional log-likelihoods of Model 3 after adding and estimating the parameters related to Hurricane Matthew.

suggests that the quantitative advantage Model 3 has over its respective benchmark is primarily due to the model's ability to describe a resurgence of cases after a department records a week of zero cholera cases. This result may be unsurprising in the context of the models that we are comparing. Because the cholera transmission in individual departments likely depends on the national prevalence of cholera and the *Vibrio cholerae* bacteria, our benchmark model that relies exclusively on the previous number of case within any given unit has a difficult time predicting a resurgence of cases.

The difference in log-likelihoods between Model 3 and its benchmark model for each individual units suggests that Model 3 has a relatively poor fit for the four units with the most sustained cholera transmission. The simple four parameter benchmark has a higher likelihood than Model 3 for the Artibonite and Nord departments, and also has log-likelihoods only a few units smaller than Model 3 for units Centre and Ouest. This is particularly worrisome given that these four departments account for more than 77% of the total number of reported cholera cases.

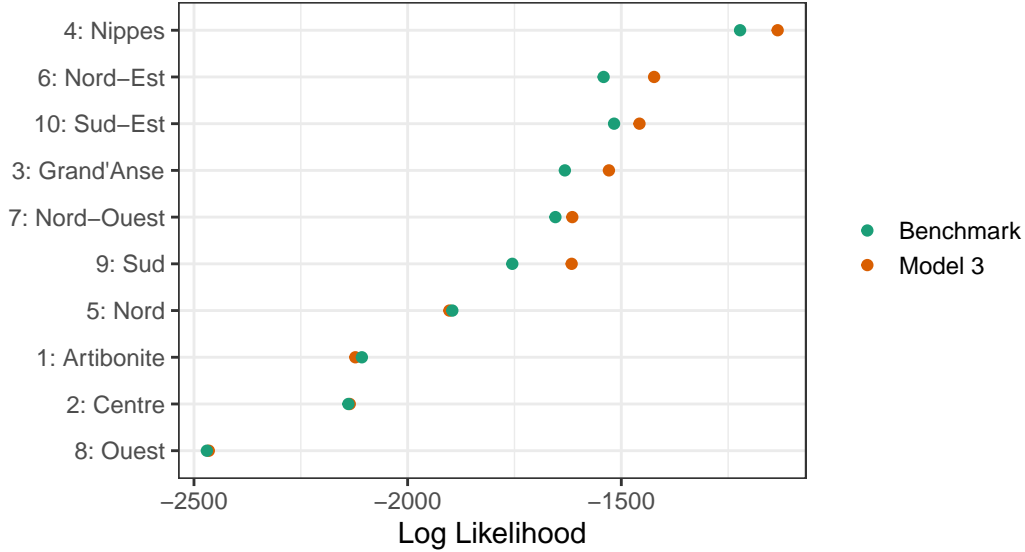


Fig S-7: Log-likelihoods of Model 3 for each department compared to the corresponding benchmark model after adding and estimating parameters related to Hurricane Matthew.

S6.1 Examining the Hidden States of the Calibrated Model

For mechanistic models, beating a suitable statistical benchmark does not alone guarantee that the model provides an accurate description of a dynamic process. Indeed, a good statistical fit does not require the model to assert a causal explanation. For example, reconstructed latent variables should make sense in the context of alternative measurements of these variables (Grad et al., 2012). We demonstrate this principle by examining the latent state of the calibrated model. In particular, we examine the compartment of susceptible individuals under various scenarios.

Recall that the filtering distribution for the calibrated version of Model 3 at time t_k is defined as the distribution of the latent state at time t_k given the data from times $t_1 : t_k$, i.e. $f_{\mathbf{X}_k | \mathbf{Y}_{1:k}}^{(3)}(\mathbf{x}_k | \mathbf{y}_{1:k}^*; \hat{\theta})$. In general, one may expect simulations from the filtering distribution of a model with a good statistical fit to result in hidden states that are highly consistent with the observed data because the filtering distribution is conditioned on the observed data. Fig. S-8 shows the percentage of individuals that are in the susceptible compartment from various simulations of the model: simulations from Model 3 under initial conditions are displayed in red; simulations from the filtering distribution of model are displayed in blue. This figure shows that simulations from initial conditions tends to result in a much more rapid depletion of susceptible individuals at the start of the epidemic than simulations from the filtering distribution, suggesting the calibrated model has a propensity to predict larger outbreaks than what is typically seen in the data. This also appears true in later stages of the time period of observed data, where the data suggests that there is a replenishment of the susceptible compartment, but the Model simulations typically retain a smaller proportion of susceptible individuals. This result demonstrates that the calibrated model favors a more rapid growth in cholera cases than what is typically seen in the observed data, which explains why the model fails to predict the absence of cases between February, 2019 and October, 2022.

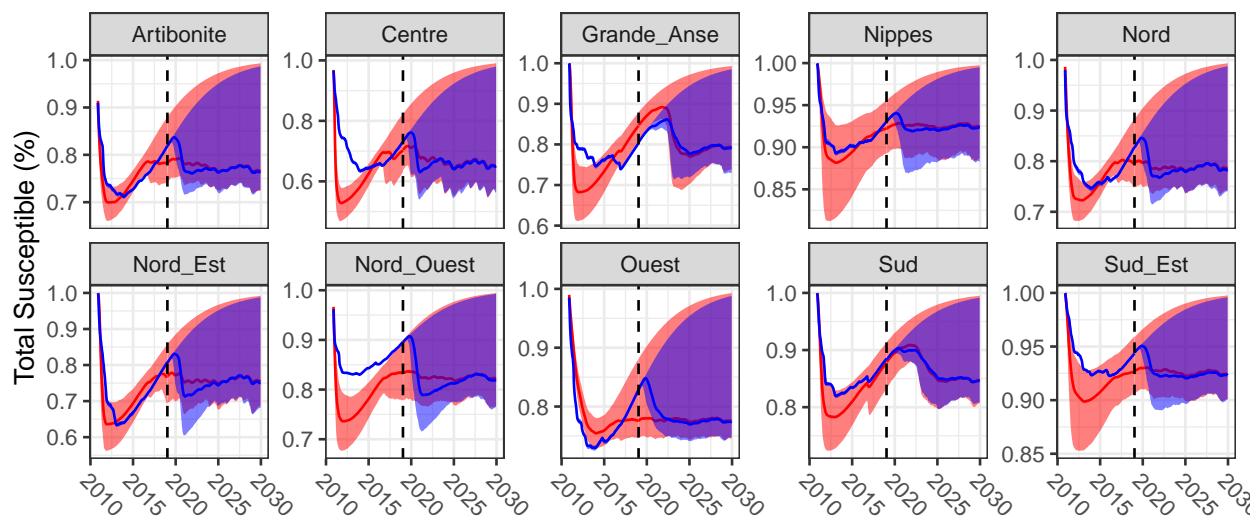


Fig S-8: Percentage of individuals that are in the susceptible compartment. Simulations from Model 3 under initial conditions are displayed in red; simulations from the filtering distribution of model are displayed in blue. The dashed line represents the end of the observed data.

S7 Replication of Lee et al. (2020a)

In this article we claimed that we were able to obtain better fits to the observed data using the same models that were proposed by Lee et al. (2020a). Along with visual comparisons to the data, this claim was supported by comparing likelihoods and AIC values in Table 2 in the manuscript. Because model likelihoods were not provided by Lee et al. (2020a), it is necessary to replicate these models in order to obtain likelihood estimates. Here we would like to thank the authors of Lee et al. (2020a), who provided detailed descriptions of their models, which enabled us to build on their work. In the following subsections, we use our R package `haitipkg` to reproduce some of the results of Lee et al. (2020a). This reproduction allows us to estimate the likelihoods of the Lee et al. (2020a) version of Models 1–3, and also provides a demonstration of the importance and usefulness of reproducible research.

S7.1 Model 1 Replication

The model was implemented by a team at Johns Hopkins Bloomberg School of Public Health (hereafter referred to as the Model 1 authors) in the R programming language using the `pomp` package (King et al., 2016). Original source code is publicly available with DOI: 10.5281/zenodo.3360991. The final results reported by the Model 1 authors were obtained by using several different parameter sets rather than a single point estimate. According to the supplement materials, this was because model realizations from a single parameter set retained substantial variability, but multiple realizations from a collection of parameter sets resulted in a reasonable visual fit to the data. We are also inclined to believe that the use of multiple parameter values was in part intended to account for parameter uncertainty—the importance of which was discussed in the main text—an effort by the Model 1 authors that we applaud. Simulations from each of the parameter sets, however, were treated with equal importance when being used to diagnose the model fit and make inference on the system. This is problematic given Figures S8 and S9 of the supplement material, which suggest that some parameter sets that were used for inference may have been several hundred units of log-likelihood lower than other parameter sets that were simultaneously used to make forecasts. Such a large difference in log-likelihoods is well beyond the threshold of statistical uncertainty determined by Wilks’ theorem, resulting in the equal use of statistically inferior parameter sets in order to make forecasts and conduct inference on the system.

To fully reproduce the results of the Model 1 authors, it is necessary to use the exact same set of model parameters that were originally used to obtain the results presented by Lee et al. (2020a). Because these parameter sets were not made publicly available, we relied on the source code provided by the Model 1 authors to approximately recreate the parameter set. Due to software updates since the publication of the source code, we were unable to produce the exact same set of parameters. Running the publicly available source code, however, resulted in a set of parameters that are visually similar to those used by the Model 1 authors (See Figures S-9 and S-10). Furthermore, simulations using the set of parameters produced by the source code appear practically equivalent to those displayed by Lee et al. (2020a) (See Figure S-11).

Because the model forecasts provided by Lee et al. (2020a) come from various sets of parameters—which each correspond to a unique log-likelihood value—it is not obvious how one would obtain an estimate for the log-likelihood of the model that was used for simulations by the Model 1 authors. One approach could be to calculate the logarithm of the weighted mean of the likelihoods for each parameter sets used to obtain the forecasts, where the weights are proportional to the number of

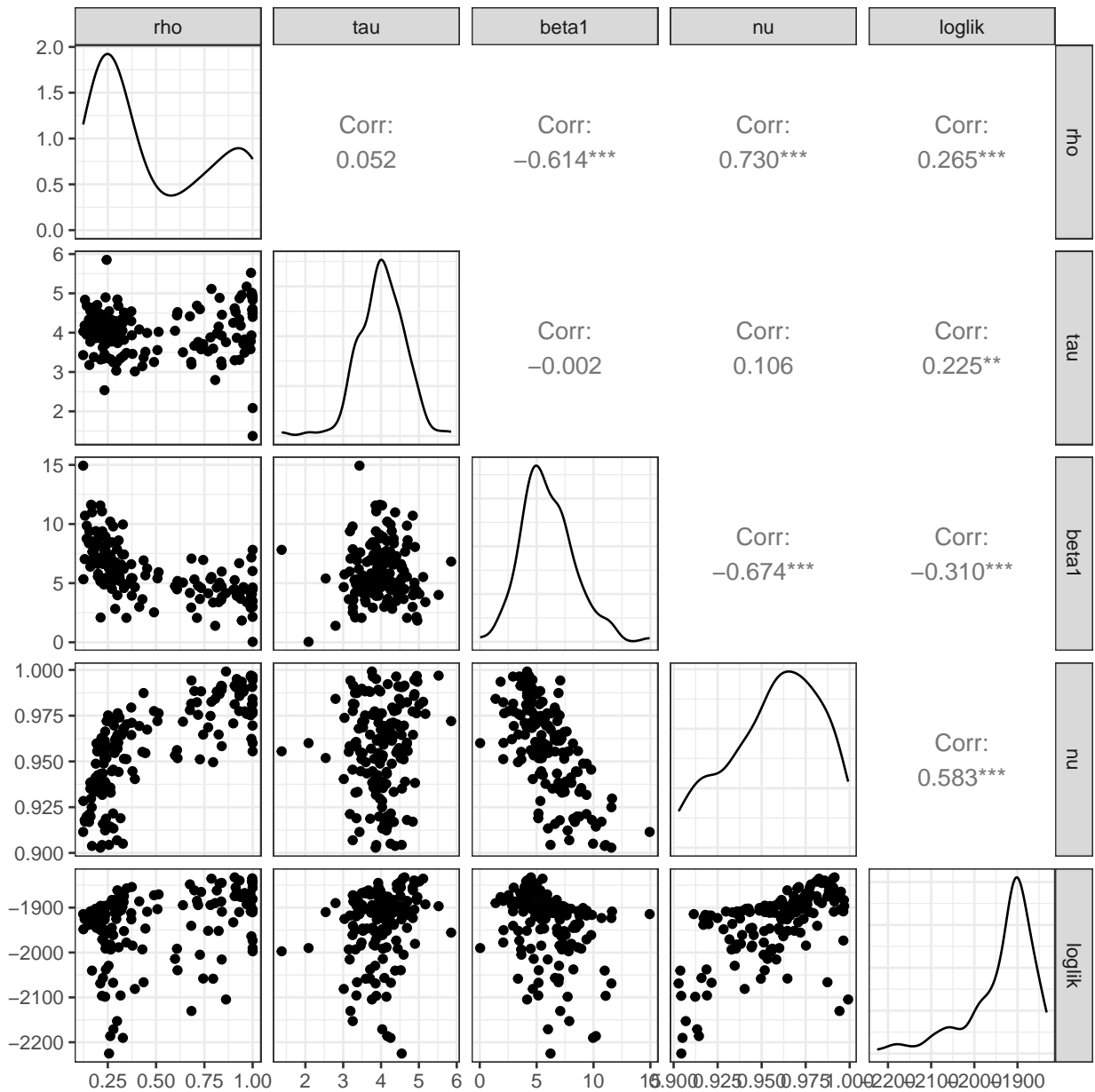


Fig S-9: Bivariate distributions of parameter estimates after fitting epidemic phase of the Model 1 following the procedure described by Lee et al. (2020). Compare to Figure S8 in the supplement of Lee et al. (2020).

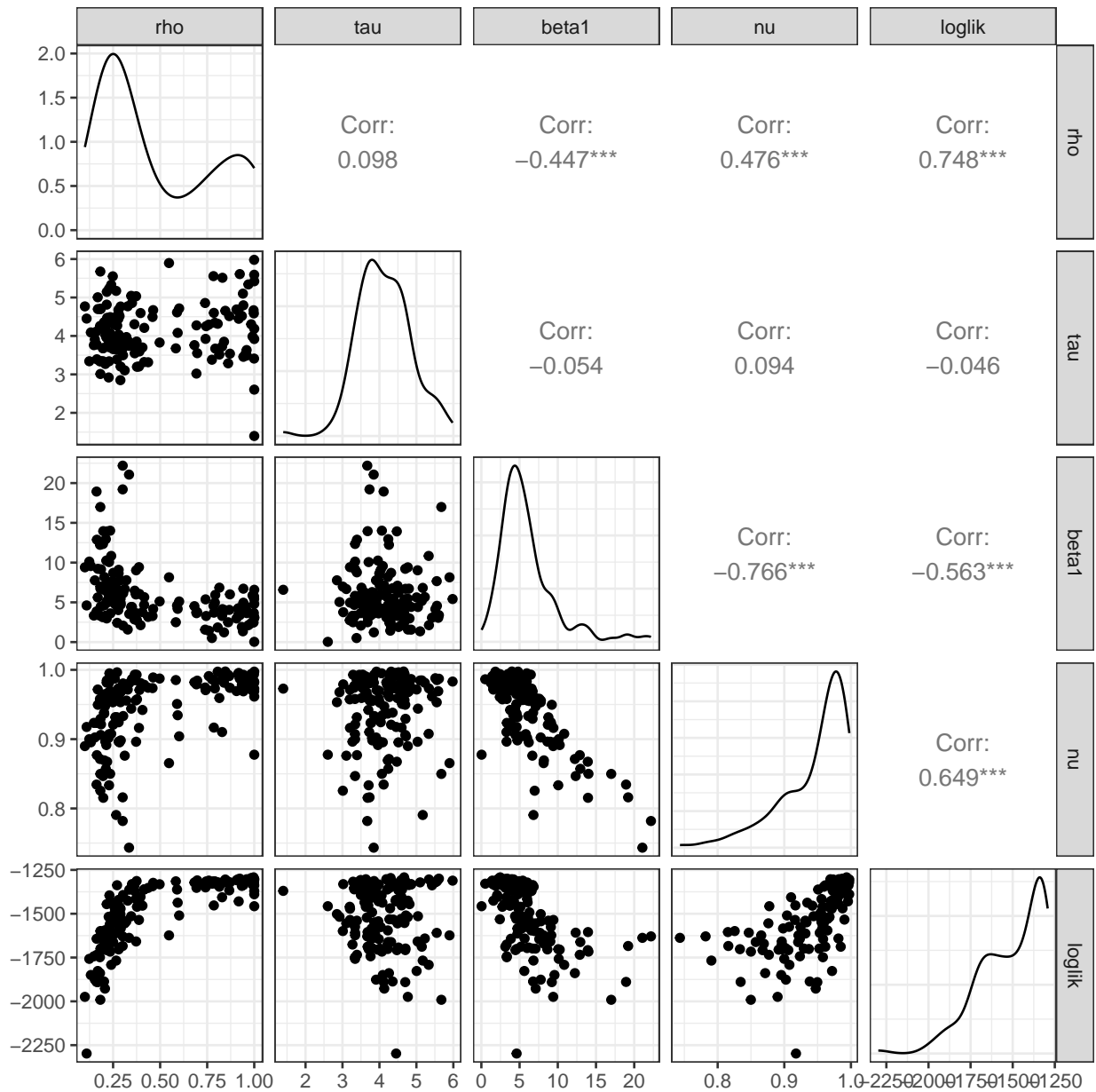


Fig S-10: Bivariate distributions of parameter estimates after fitting endemic phase of the Model 1 following the procedure described by Lee et al. (2020). Compare to Figure S9 in the supplement of Lee et al. (2020).

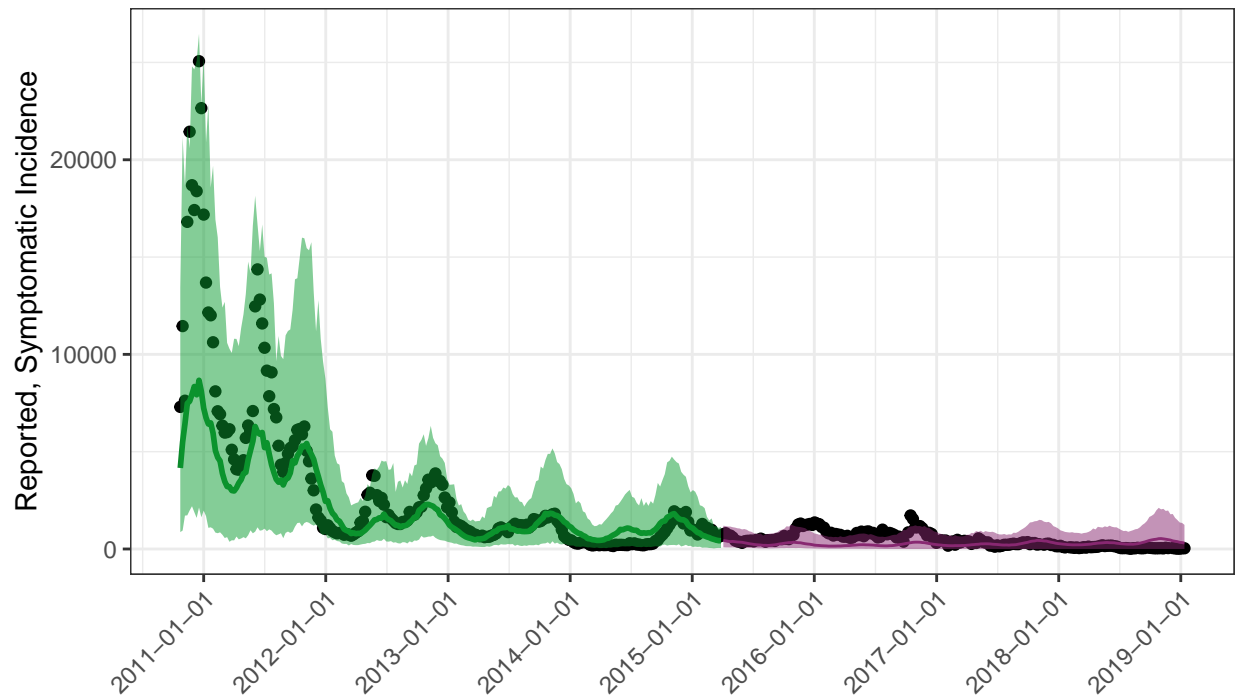


Fig S-11: Simulations using parameter sets that were generated by running source code provided by Lee et al (2020). Compare to Figure S7 in the supplement of Lee et al. (2020). The upper bound for the likelihood of this model is -3031.

times the parameter set was used. However, in an effort to not underestimate the likelihood of the model of the Model 1 authors, we report the estimated log-likelihood as the log-likelihood value corresponding to the parameter set with the largest likelihood value, even though the majority of simulations were obtained using parameter sets with lower likelihood values. In this sense, we consider the log-likelihood reported in Table 1 of the main text to be an upper-bound of the log-likelihood of the model used by Lee et al. (2020a). For each parameter set, the log-likelihood was estimated using a particle filter, implemented as the `pfilter` function in the `pomp` package.

S7.2 Model 2 Replication

Model 2 was developed by a team that consisted of members from the Fred Hutchinson Cancer Research Center and the University of Florida (hereafter referred to as the Model 2 authors). While Model 2 is the only deterministic model we considered in our analysis, it contains perhaps the most complex descriptions of cholera in Haiti: Model 2 accounts for movement between spatial units; human-to-human and environment-to-human cholera infections; and transfer of water between spatial units based on elevation charts and river flows.

The source code that the Model 2 authors used to generate their results was written in the Python programming language, and is publicly available at [10.5281/zenodo.3360857](https://zenodo.org/record/3360857) and its accompanying GitHub repository <https://github.com/lulelita/HaitiCholeraMultiModelingProject>. In order to perform our analysis in a unified framework, we re-implemented this model in the R programming language using the `spatPomp` package (Asfaw et al., 2023), which facilitates the creation of meta-population models. We note that the travel and water matrices used to implement the complex dynamics in Model 2 (Lee et al., 2020b) are not available in either the Zenodo archive or the GitHub repository; instead, we obtained these matrices via personal correspondence with the Model 2 authors. Using these matrices, and the point estimates for model parameters provided by (Lee et al., 2020b), we created trajectories of the cholera dynamics and compared this to available data. These trajectories, shown in Figure S-12, are very similar to the trajectories shown in Figure S15 of Lee et al. (2020b).

There are minor differences between Figure S-12 and Figure S15 of Lee et al. (2020b). While the discrepancy appears minor, the deterministic nature of Model 2 implies that an exact replication of model trajectories should be possible. In this case, these discrepancies may possibly be attributed to implementing the model and plotting the model trajectory in two different programming languages. Another potential explanation for the discrepancy is that the parameters that we used are only approximately the same as those used by Lee et al. (2020b). For example, the parameters β , β_W (See Table S-1) had reported values of 9.9×10^{-7} and 4.03×10^{-2} , respectively (Table S13 of Lee et al. (2020b)), but were actually fit to data and therefore likely these values have been rounded. Additionally, our implementation of Model 2 used a time scale of years and many of the parameters were reported on a weekly scale, so small differences may result due to unit conversions. The collective effect of these small differences in model parameters likely will result in small differences in model trajectories.

Some additional concerns about being able to accurately replicate the results of Lee et al. (2020a) are valid. Details about the measurement models and how latent states were initialized for the epidemic model were not provided by Lee et al. (2020b) and therefore these details must be inferred by looking at the provided source code. According to repository comments, the files `fitInPieces3paramsCleanMay2019Public.py` and `fitInPiecesMuWithFracSusFixedAllInfectionsPublic.py` were used to fit the epidemic and endemic phases of the model respectively,

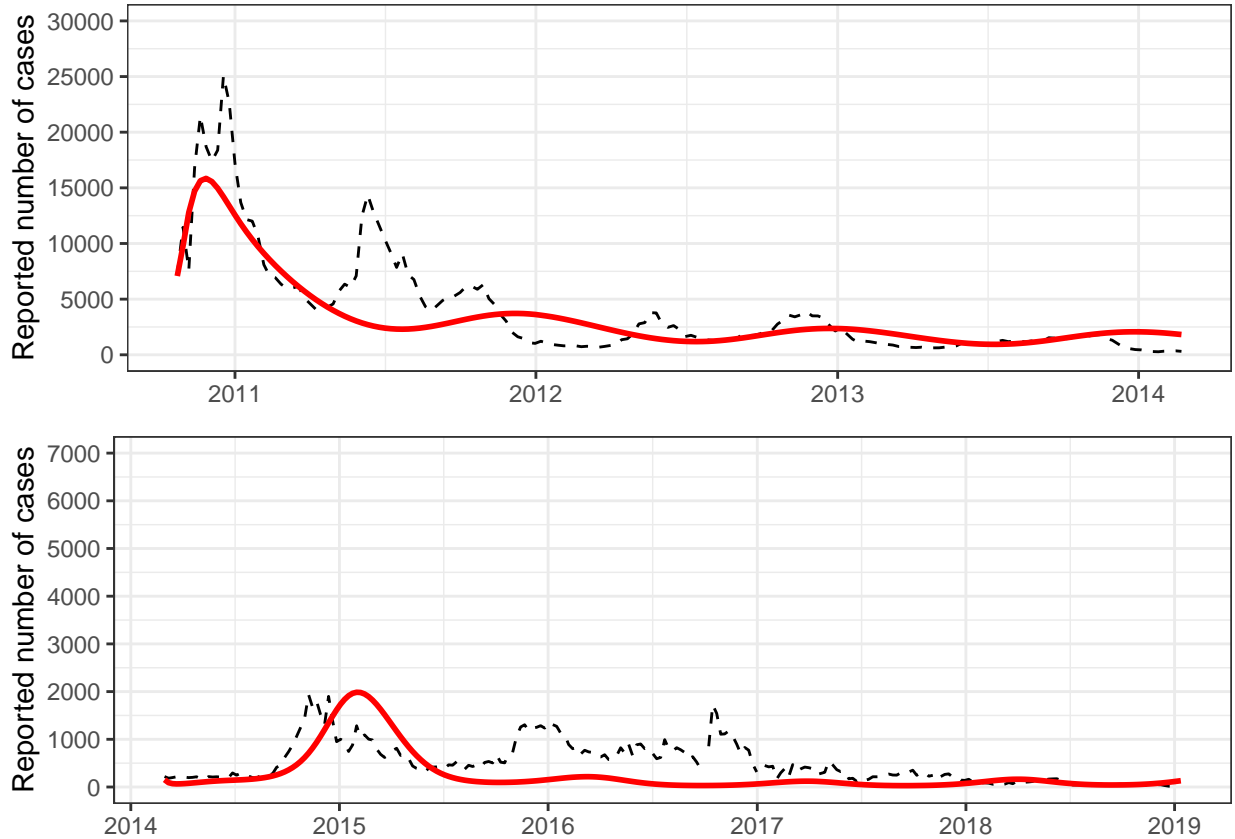


Fig S-12: Model 2 trajectories using the `haitipkg`. Compare to Figure S15 in the supplement of Lee et al. (2020b).

although it is apparent that these exact files were not used to obtain the reported results since the files contain some variable-naming errors that make it impossible to run the files without making modifications¹. The inability to replicate the results by Lee et al. (2020a) by running the provided source code makes checking whether or not our numeric implementation faithfully represents their results very difficult. Additionally, the script that was said to be used to obtain the results reported by Lee et al. (2020a) appears to use a different measurement model than what was described in the supplemental material, again making it difficult to fully replicate the result of Lee et al. (2020a) without being able to easily run the provided source code. In this case, we chose to use measurement model described by Eq. S17 for both phases of the epidemic, as this seemed to visually match the results of Lee et al. (2020a) most closely.

S7.3 Model 3 Replication

Model 3 was developed by a team of researchers at the Laboratory of the Swiss Federal Institute of Technology in Lausanne, hereafter referred to as the Model 3 authors. The code that was

¹One example of why the code cannot be run that the file loads functions from a non-existent file named `choleraEqs.py` in line 13 rather than `choleraEqsPublic.py`.

originally used to implement Model 3 is archived with the DOI: 10.5281/zenodo.3360723, and also available in the public GitHub repository: jcblemait/haiti-mass-ocv-campaign. Because the code was made publicly available, and final model parameters were reported in the supplementary material of Lee et al. (2020a), we were able to reproduce Model 3 by directly using the source code. In Fig. S-13, we plot simulations from this model. This figure can be compared to Figure S18 of Lee et al. (2020a). We note that slight differences may be accounted for due to variance in the model simulations and the difference in programming language used to produce the figure. Overall, the high standard of reproducibility that was achieved by the Model 3 authors facilitated the ability to readily replicate their model and results.

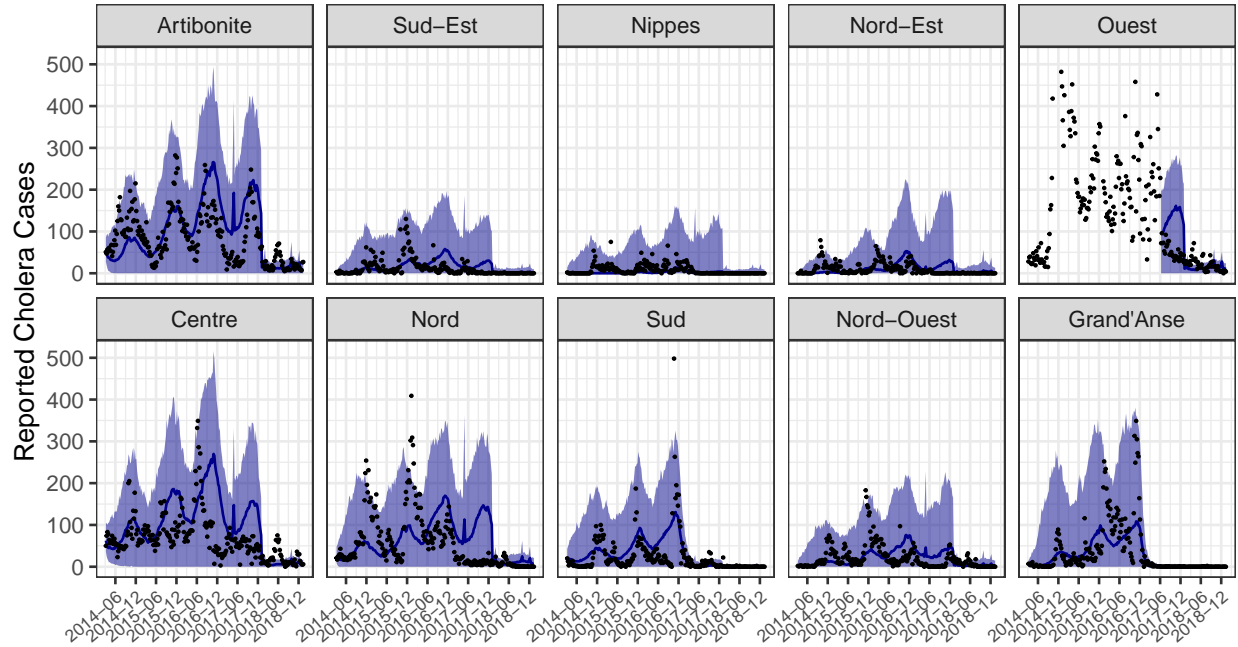


Fig S-13: Simulations from Model 3. Compare to Figure S18 in the supplement of Lee et al. (2020a).

S8 Forecasting with parameter uncertainty

Let $f_{Y_{1:N}}(y_{1:N}|\theta)$ denote the pdf of the model under consideration, where θ is a parameter vector that indexes the model. Furthermore, denote the observed data as $y_{1:N}^*$. Because the uncertainty in just a single parameter can lead to drastically different forecasts (Saltelli et al., 2020), parameter uncertainty should be considered when obtaining model forecasts when the goal is to influencing policy. In a Bayesian modelling paradigm, the most natural way to account for parameter uncertainty in model forecasts is to suppose that θ comes from a distribution f_{Θ} , and then to obtain J forecasts from the model where each forecast is obtained using parameters drawn from the posterior distribution $\Theta_{1:J} | Y_{1:N} = y_{1:N}^* \sim f_{\Theta}(\theta | Y_{1:N} = y_{1:N}^*)$.

When frequentist methods are used, however, there does not exist a posterior distribution from which one could sample. A common approach could be to obtain a weighted average of the

simulations from various models (Hoeting et al., 1999), but this can be problematic when forecasts from each model are very different from each other (Grueber et al., 2011). A similar approach that has been taken (King et al., 2015) is to obtain model forecasts using multiple sets of parameter values and then sample from the resulting forecasts using weights proportional to the corresponding likelihoods of the parameter values. This approach could be considered as empirical Bayes, as it is equivalent to using a discrete uniform prior where the set of values in the prior distribution is determined by a stochastic routine applied to the observed data, as discussed below.

For each $i \in 1 : k$, let Θ_i be a random vector of model parameters. Then, letting Θ denote the true model parameters, we endow the set $\{\Theta_1, \Theta_2, \dots, \Theta_k\}$ with a discrete uniform distribution, such that $P(\Theta = \Theta_i) = \frac{1}{K}$ for all values $i \in 1 : k$. Using this as a prior distribution, the posterior distribution of $\Theta | Y_{1:N} = y_{1:N}^*$ can be expressed as: $P(\Theta = \Theta_k | Y_{1:N} = y_{1:N}^*) = \frac{f_{Y_{1:N}}(y_{1:N}^* | \Theta_k)}{\sum_{l=1}^K f_{Y_{1:N}}(y_{1:N}^* | \Theta_l)}$. In a standard empirical Bayes analysis, the values $\Theta_1, \dots, \Theta_k$ of the prior distribution would be chosen using the observed data, resulting in a posterior distribution that weighs the prior parameter vectors proportional to their corresponding likelihoods. Instead, we choose Θ_i to be the output of a stochastic routine applied to the observed data by setting Θ_i to be the output of an iterated filtering algorithm. In practice, because the likelihood maximization routines of iterated filtering methods are stochastic, it is common to run the iterated filtering method multiple times for each model in order to obtain a maximum likelihood estimate for model parameters. This results in a natural set of parameters near the MLE that could be used as the discrete prior distribution.

S9 Translating to Lee et al. (2020a) notation

Since the models of Lee et al. (2020a) were developed independently, the choice of notation varies inconsistently between models. For our reanalysis, we rename parameters to provide a unified notation facilitating comparison between models. Table S-1 maps this notation back to the original notations, for reference.

Parameter	Our Notation	Lee et al. (2020a)		
		1	2	3
Reporting Rate	ρ	ρ	ρ	ϵ_1, ϵ_2
Mixing Coefficient	ν	ν	—	—
Measurement Over-Dispersion	ψ	τ	—	p
Birth Rate	μ_S	μ	—	—
Natural Mortality Rate	δ	δ	—	μ
Cholera Mortality Rate	δ_C	—	—	α
Latent Period	$1/\mu_{EI}$	$1/\sigma$	$1/\gamma_E$	—
Recovery Rate	μ_{IR}	γ	γ	γ
Loss of Immunity	μ_{RS}	α	σ	ρ
Symptomatic Ratio	f	$1 - \theta_0$	k	σ
Asymptomatic Relative Infectiousness	ϵ	κ	red_β	—
Human-to-Water Shedding	μ_W	—	μ	θ_I
Asymptomatic Relative Shedding	ϵ_W	—	red_μ	θ_A/θ_I
Seasonal Amplitude	a	—	α_s	λ
Transmission	β	β	β	c
Water-to-Human	β_W	—	β_W	β
Bacteria Mortality	δ_W	—	δ	μ_β
Vaccination Efficacy	θ	θ_{vk}	$\theta_1, \theta_2, \theta_{15}, \theta_{25}$	η_{1d}, η_{2d}
Process Over-dispersion	σ_{proc}	—	—	σ_w

Table S-1: Translations between our common notation and notation used by Lee et al (2020).

Supplementary References

- Asfaw, K., Park, J., King, A. A., and Ionides, E. L. (2023). Partially observed Markov processes with spatial structure via the R package spatPomp. *arXiv:2101.01157v3*.
- Barzilay, E. J., Schaad, N., Magloire, R., Mung, K. S., Boncy, J., Dahourou, G. A., Mintz, E. D., Steenland, M. W., Vertefeuille, J. F., and Tappero, J. W. (2013). Cholera surveillance during the Haiti epidemic—the first 2 years. *New England Journal of Medicine*, 368(7):599–609. Includes case definition to 2013: The NCSS used a modified World Health Organization case definition for cholera that included acute watery diarrhea, with or without vomiting, in persons of all ages residing in an area in which at least one case of *Vibrio cholerae* O1 infection had been confirmed by culture.
- Bhadra, A., Ionides, E. L., Laneri, K., Pascual, M., Bouma, M., and Dhiman, R. C. (2011). Malaria in Northwest India: Data analysis via partially observed stochastic differential equation models driven by Lévy noise. *Journal of the American Statistical Association*, 106:440–451.
- Bretó, C., He, D., Ionides, E. L., and King, A. A. (2009). Time series analysis via mechanistic models. *Annals of Applied Statistics*, 3:319–348.
- Bretó, C. and Ionides, E. L. (2011). Compound Markov counting processes and their applications to modeling infinitesimally over-dispersed systems. *Stochastic Processes and their Applications*, 121:2571–2591.
- Ferreira, S. (2016). Cholera threatens Haiti after Hurricane Matthew. *BMJ*, 355:i5516.
- Grad, Y. H., Miller, J. C., and Lipsitch, M. (2012). Cholera modeling: Challenges to quantitative analysis and predicting the impact of interventions. *Epidemiology*, 23(4):523.
- Grueber, C. E., Nakagawa, S., Laws, R. J., and Jamieson, I. G. (2011). Multimodel inference in ecology and evolution: challenges and solutions. *Journal of Evolutionary Biology*, 24(4):699–711.
- He, D., Ionides, E. L., and King, A. A. (2010). Plug-and-play inference for disease dynamics: Measles in large and small towns as a case study. *Journal of the Royal Society Interface*, 7:271–283.
- Hoeting, J. A., Madigan, D., Raftery, A. E., and Volinsky, C. T. (1999). Bayesian model averaging: a tutorial (with comments by M. Clyde, David Draper and E. I. George, and a rejoinder by the authors. *Statistical Science*, 14(4):382 – 417.
- Ionides, E. L., Ning, N., and Wheeler, J. (2022). An iterated block particle filter for inference on coupled dynamic systems with shared and unit-specific parameters. *Statistica Sinica*,, pages pre-published online.
- King, A. A., Domenech de Cellès, M., Magpantay, F. M., and Rohani, P. (2015). Avoidable errors in the modelling of outbreaks of emerging pathogens, with special reference to ebola. *Proceedings of the Royal Society B: Biological Sciences*, 282(1806):20150347.
- King, A. A., Nguyen, D., and Ionides, E. L. (2016). Statistical inference for partially observed Markov processes via the R package pomp. *Journal of Statistical Software*, 69:1–43.

- Lee, E. C., Chao, D. L., Lemaitre, J. C., Matrajt, L., Pasetto, D., Perez-Saez, J., Finger, F., Rinaldo, A., Sugimoto, J. D., Halloran, M. E., Longini, I. M., Ternier, R., Vissieres, K., Azman, A. S., Lessler, J., and Ivers, L. C. (2020a). Achieving coordinated national immunity and cholera elimination in Haiti through vaccination: A modelling study. *The Lancet Global Health*, 8(8):e1081–e1089.
- Lee, E. C., Chao, D. L., Lemaitre, J. C., Matrajt, L., Pasetto, D., Perez-Saez, J., Finger, F., Rinaldo, A., Sugimoto, J. D., Halloran, M. E., Longini, I. M., Ternier, R., Vissieres, K., Azman, A. S., Lessler, J., and Ivers, L. C. (2020b). Supplement to: Achieving coordinated national immunity and cholera elimination in Haiti through vaccination: A modelling study. *The Lancet Global Health*, 8(8):e1081–e1089.
- Ning, N. and Ionides, E. L. (2021). Iterated block particle filter for high-dimensional parameter learning: Beating the curse of dimensionality. *arXiv:2110.10745*.
- Romero-Severson, E., Volz, E., Koopman, J., Leitner, T., and Ionides, E. (2015). Dynamic variation in sexual contact rates in a cohort of HIV-negative gay men. *American Journal of Epidemiology*, 182:255–262.
- Saltelli, A., Bammer, G., Bruno, I., Charters, E., Di Fiore, M., Didier, E., Nelson Espeland, W., Kay, J., Lo Piano, S., Mayo, D., Pielke, R., Portaluri, T., Porter, T. M., Puy, A., Rafols, I., Ravetz, J. R., Reinert, E., Sarewitz, D., Stark, P. B., Stirling, A., van der Sluijs, J., and Vineis, P. (2020). Five ways to ensure that models serve society: a manifesto. *Nature*, 582:428–484.
- Stocks, T., Britton, T., and Höhle, M. (2020). Model selection and parameter estimation for dynamic epidemic models via iterated filtering: Application to rotavirus in Germany. *Biostatistics*, 21(3):400–416.
- Subramanian, R., Romeo-Aznar, V., Ionides, E., Codeço, C. T., and Pascual, M. (2020). Predicting re-emergence times of dengue epidemics at low reproductive numbers: DENV1 in Rio de Janeiro, 1986–1990. *Journal of the Royal Society Interface*, 17(167):20200273.